Lattice Dirac fermions on a simplicial Riemannian manifold

Richard C. Brower, Evan S. Weinberg, George T. Fleming, Andrew D. Gasbarro, Timothy G. Raben, and Chung-I Tan

Lattice Dirac Fermions on a Simplicial Riemannian Manifold

Richard C. Brower* and Evan S. Weinberg†
Boston University, Boston, MA 02215

George T. Fleming‡ and Andrew D. Gasbarro§
Yale University, Sloane Laboratory, New Haven, CT 06520

Timothy G. Raben¶
Brown University, Providence, RI 02912 and
University of Kansas, Lawrence, KS 66047

Chung-I Tan**
Brown University, Providence, RI 02912

The lattice Dirac equation is formulated on a simplicial complex which approximates a smooth Riemann manifold by introducing a lattice vierbein on each site and a lattice spin connection on each link. Care is taken so the construction applies to any smooth D-dimensional Riemannian manifold that permits a spin connection. It is tested numerically in 2D for the projective sphere $\mathbb{S}^2$ in the limit of an increasingly refined sequence of triangles. The eigenspectrum and eigenvectors are shown to converge rapidly to the exact result in the continuum limit. In addition comparison is made with the continuum Ising conformal field theory on $\mathbb{S}^2$. Convergence is tested for the two point, $\langle \epsilon(x_1)\epsilon(x_2) \rangle$, and the four point, $\langle \sigma(x_1)\epsilon(x_2)\epsilon(x_3)\sigma(x_4) \rangle$, correlators for the energy, $\epsilon(x) = i\bar{\psi}(x)\psi(x)$, and twist operators, $\sigma(x)$, respectively.

I. INTRODUCTION

Lattice gauge theory on hypercubic lattices [1] provides a powerful *ab initio* approach to strongly coupled field theories in flat Euclidean space, $\mathbb{R}^D$. However there is important non-perturbative physics that would benefit from the extension of lattice field theory methods to more general curved Riemann manifolds. One example is a recent proposal to implement radial quantization for conformal field theories [2–4]. This requires replacing the flat Euclidean manifold, $\mathbb{R}^D$, by the cylinder, $\mathbb{R} \times \mathbb{S}^{D-1}$, which represents the boundary of Anti-de Sitter space AdS^{D+1} in global coordinates. Other examples include *ab initio* calculations of the c and a terms, tests of AdS/CFT duality, quantum criticality in condensed matter and perhaps quantum physics near blackholes.

The conventional lattice regulator in flat space is a sequence of hypercubic lattices on a torus, $\mathbb{T}^D$, with a uniform lattice spacing a, representing an increasingly larger subgroup of translations as the cut-off, $\Lambda_{UV} = \pi/a$, is removed. Curved manifolds lack such uniform sequences of lattices. For example, on a sphere, the finest uniform discretization of $\mathbb{S}^2$ and $\mathbb{S}^3$ are the 20-cell icosahedron and the 600-cell tetraplex respectively. The lack of an infinite sequence of regular lattices approaching the continuum compounds the problem of renormalization and

* brower@bu.edu
† weinbe2@bu.edu
‡ george.fleming@yale.edu
§ andrew.gasbarro@yale.edu
¶ timothy.raben@ku.edu
** chung-i_tan@brown.edu

symmetry restorations as the cut-off is removed. This paper is part of research to develop a general strategy [5], referred to as Quantum Finite Elements (**QFE**), to formulate a lattice field theory path integral for any renormalizable quantum field theory on a smooth Riemann manifold $(\mathcal{M}, g)$ given the target metric tensor, $g_{\mu\nu}(x)$. Here we focus on the construction of the free lattice Dirac fermion. The fermion is an especially challenging and interesting example. The spinor probes the underlying geometry of the manifold through its vierbein and spin connection. From the perspective of Regge Calculus [6], the vierbein and spin connection are sufficient to define a simplicial manifold in the Einstein-Cartan formulation of lattice gravity [7]. Consequently the fermion lattice field may also provide an alternative approach to reconstructing the intrinsic geometry for the Regge Calculus approximation to the base Riemann manifold.

The organization of the paper is as follows. In Sec. II, to establish our notation and basic formalism, we review the Finite Element approximation to scalar field theory on a Riemann manifold. While we borrow heavily from the conventional piecewise linear form for Regge Calculus (RC) and Finite Element Method (FEM), it is important to note that these approximations do not by themselves adequately address our problem. (Readers familiar with finite elements may prefer to first skip this introduction and return for notation.) In Sec. III, we begin the construction for the Dirac field, emphasizing the new problem of defining the lattice vierbein and spin connection and removing doublers on the simplicial complex. In Sec. IV we formulate an algorithm for fixing the lattice vierbein and spin connection designed to converge to any target smooth Riemann manifold $(\mathcal{M}, g)$. In Sec. V

we test the method for the Dirac fermion and its rate of convergence for the $\mathbb{S}^2$ sphere compared to the exact continuum theory. In Sec. VI the simplicial Majorana fermion on $\mathbb{S}^2$ is shown to converge to the analytical result for 2-point and 4-point correlation functions for the c = 1/2 minimal model conformal field theory. In Sec. VII we discuss extensions and future directions in the study of quantum field theories with gauge and scalar fields. Several technical details are relegated to the appendices.

II. REVIEW OF SCALAR FIELDS ON A SIMPLICIAL LATTICE

Lattice field theory on a Riemann manifold $(\mathcal{M}, g)$ requires a discrete definition for the metric field, $g_{\mu\nu}(x)$, and the quantum fields, scalars $\phi(x)$, fermions $\psi(x)$, and gauge fields $A_\mu(x)$. Aspects of this problem have been considered extensively in a number of related fields. One example is Regge Calculus (RC), which introduces an ensemble of piecewise flat simplicial lattices as a basis for non-perturbative quantum gravity [6]. A second example is FEM, designed to discretize partial differential equations and to solve them numerically [8]. The third example involves a formal geometrical framework [9] for a Discrete Exterior Calculus (DEC) on the Delaunay lattice $\mathcal{S}$ and its circumcenter Voronoi dual $\mathcal{S}^*$. We should also emphasize the classic study of field theory on random lattices by Christ, Friedberg and Lee (CFL) [10–12] that in fact anticipated much of the relevant FEM and DEC formalism for the simplicial lattice field theory in flat space.

Each method provides some useful and closely related tools, but they do not fully address the problems of a rigorous simplicial lattice representation guaranteed to converge to the continuum for renormalizable quantum field theories—the ultimate goal of this research. Both the RC and the CFL approaches introduce a random ensemble of simplicial lattices in order to hopefully restore continuum symmetries (diffeomorphisms, chiral symmetry, etc.) of the target quantum field theory. Here we do not advocate this approach. **Instead we impose regularity on a single sequence of increasingly refined simplicial lattices designed to approach the continuum limit on a fixed target Riemann manifold.** Our approach depends on combining two elements. First the **classical** FEM method provides the theoretical framework of convergence [8] in the IR for all solutions to the equation of motion (EOM or PDEs) smooth enough to be insensitive to the UV cutoff. Second, counter terms are added to the FEM Lagrangian to deal with the UV divergences so that the lattice quantum path integral will converge to the target renormalizable quantum field theory on the Riemannian manifold. We refer to the combination of these two steps as the **Quantum Finite Element** (QFE) method. While the problem of UV divergences is not addressed here, the reader is referred to a companion article [13], where the one loop

QFE counter term is successfully applied to the 2D ϕ^4 theory on $\mathbb{S}^2$ at the Wilson-Fisher conformal fixed point.

A. Piecewise Linear Finite Elements

Consider the action for a free scalar field in the continuum on $(\mathcal{M}, g)$ given by

$$S = \frac{1}{2} \int_{\mathcal{M}} d^D x \sqrt{g} \left[g^{\mu\nu} \partial_\mu \phi(x) \partial_\nu \phi(x) \right.$$
$$\left. + (m^2 + \xi R)\phi^2(x) \right] , \qquad (1)$$

with proper distances defined by the metric,

$$ds^2 = g_{\mu\nu}(x) dx^\mu dx^\nu , \qquad (2)$$

and its determinant, $g = \det(g_{\mu\nu})$. Assume also that the Riemann manifold is **torsion free** ($\Gamma^\lambda_{\mu\nu} = \Gamma^\lambda_{\nu\mu}$) and **metric compatible** ($\nabla_\rho g_{\mu\nu} = 0$) so the Levi-Civita connection is determined uniquely in terms of the metric,

$$\Gamma^\lambda_{\nu\mu} = \frac{1}{2} g^{\lambda\rho} (\partial_\mu g_{\nu\rho} + \partial_\nu g_{\mu\rho} - \partial_\rho g_{\mu\nu}) . \qquad (3)$$

The classical action (1) is diffeomorphism invariant. The coupling $\xi = (D-2)/(4(D-1))$ to the Ricci scalar curvature is required for conformal invariance at zero mass but henceforth we will set the Recci scalar term (1) to zero since it is inessential for this FEM review.

The conventional FEM/Regge Calculus approach to a simplicial approximation can be broadly broken into three steps.

- **Topology:** The D-dimensional target manifold $\mathcal{M}$ is replaced by a simplicial complex $\mathcal{M}_\sigma$ composed of elementary D-simplices, which is homeomorphic to the target manifold.

- **Geometry:** The metric on the target manifold $(\mathcal{M}, g)$ is approximated on the simplicial complex to form a "lattice Riemann manifold" $(\mathcal{M}_\sigma, g_\sigma)$ by assigning lengths l_{ij} on links and extending the metric into the interior of each simplex with piecewise flat volumes.

- **Hilbert Space:** The Hilbert space of continuum fields, $\phi(x)$, is truncated by expanding in a finite element basis on each simplex, $\phi_\sigma(x) \simeq \sum_{i=0}^{D} E^i(x) \phi_i$.

In principle one can construct a one-to-one map between points on the target smooth Riemann manifold $(\mathcal{M}, g(x))$ and points on the piecewise flat simplicial manifold $(\mathcal{M}_\sigma, g_\sigma(y))$ introduced in Regge Calculus [6] that preserves distance to order $O(a^2)$, where the *lattice spacing*, a, is a bound on the simplicial diameters. There are two approaches to this map, employed in detail in Sec IV: The first approach uses the intrinsic geometry of the D-dimensional manifold, and the second a higher

dimensional embedding in flat Euclidean space $\mathbb{R}^N$ for $N > D$.

The first approach is more fundamental. One chooses a collection of points x_i in $\mathcal{M}$ and constructs a simplicial complex for this set. A discrete metric in the spirit of Regge Calculus is computed by an approximation l_{ij} to the geodesic distances on each link $\langle i, j \rangle$. Then each D-simplex is interpolated by piecewise flat co-ordinates y. In general, there are subtleties involved in achieving a good approximation. The geodesics are only unique if neighboring points are sufficiently close. An optimal triangulation should use the Voronoi construction which requires a reasonable approximation to the distances. (Note that Regge Calculus avoids this problem by reversing the logic. The simplicial manifold is assumed to be given *a priori* with the target manifold as a consequence defined in the continuum limit, $l_{ij} = O(a) \to 0$.)

The second and much easier approach, when it is available, is to start with an isometric embedding of the D-dimensional Riemann manifold $(\mathcal{M}, g)$ into a higher dimensional flat Euclidean space $\mathbb{R}^N$. An important example is the $\mathbb{S}^D$ sphere discussed in Sec. IV C . This is easily embedded as $\vec{r} \in \mathbb{R}^{D+1}$ such that $\vec{r} \cdot \vec{r} = R_0^2$ with R_0 fixed. Then one uses a Voronoi construction of simplices on a set of discrete sites at $x = r_i$ assigning the Euclidean distances, $l_{ij} = |r_i - r_j|$, to the edges. This construction turns out to be invariant under the projective transformation of the sphere $\mathbb{S}^D$ to the plane $\mathbb{R}^D$. In general, if we can find a smooth isometric embedding, this will guarantee convergence of the simplicial manifold $(\mathcal{M}_\sigma, g_\sigma)$ to the target manifold $(\mathcal{M}, g)$ as $a \to 0$.

To approximate the Hilbert space, we can expand the field ϕ_σ in a local FEM basis [8]. Properly constructed this convergences to the continuum field, $|\phi_\sigma(x) - \phi(x)| \to 0$, as the diameters a of all simplicial elements vanish. But more importantly, FEM theorems also impose precise *shape regular* condition [8] on the simplicial geometry to guarantee that all solutions of discrete equations of motion (EOM) converge to the classical solutions of the continuum EOM. This is a subtle theoretical problem, which involves the order of the differential equation, the non-linearities of the PDEs, boundary conditions, the choice of FEM basis, etc. For free fermions, even in flat space, there are additional well known difficulties, not addressed in the FEM literature to our knowledge, due to the notorious spectrum doubling problem and the need to restore chiral symmetry.

Simplicial Geometry and Notation: It is helpful to understand a bit of the formal aspects of each step listed above in order to establish notation. One builds up the lattice field theory representation in layers: start with the simplicial complex $\mathcal{S}$, then add a metric to get the Regge Calculus, and lastly add matter fields to construct the simplicial action for the quantum field theory. The shared topological and algebraic properties mapped between each abstract layer is the province of *Category theory* [14].

A pure simplicial complex $\mathcal{S}$ consists of a set of D-
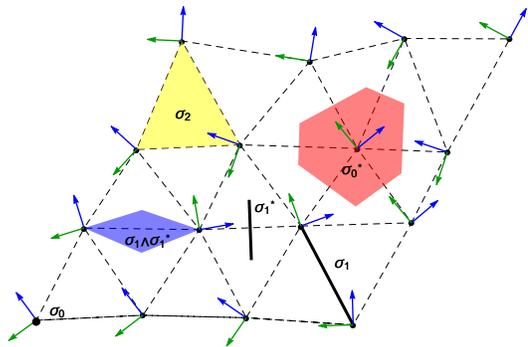
FIG. 1. A 2D simplicial complex with points (σ_0), edges (σ_1) and triangles (σ_2). At each vertex σ_0 there is a dual polytope in σ_0^* (illustrated in red), and at each link, σ_1, there is a dual link σ_1^* and its associated hybrid cell $\sigma_1 \wedge \sigma_1^*$ (illustrated in blue). The arrows at each site represent a random basis for the local tangent plane.

dimensional simplices (designated by σ_D) "glued" together at shared faces (boundaries) consisting of $D-1$ dimensional simplices (σ_{D-1}). The D-dimensional simplex is built iteratively from lower dimensional simplices,

$$\sigma_0 \to \sigma_1 \to \sigma_2 \to \cdots \to \sigma_D , \qquad (4)$$

beginning with $D+1$ sites $\sigma_0(i)$ with $i = 0, 1, \cdots, D$ on each simplex, connected together by $(D+1)D/2$ directed links $\sigma_1(i_1 i_2) \equiv \langle i_1, i_2 \rangle$ forming $D(D+1)(D+2)/3!$ oriented triangles $\sigma_1(i_1 i_2 i_3) \equiv \triangle_{i_1 i_2 i_3}$, etc. This hierarchy is specified by the boundary operator,

$$\partial \sigma_n(i_0 i_1 \cdots i_n) = \sum_{k=0}^{n} (-1)^k \sigma_{n-1}(i_0 i_1 \cdots \widehat{i}_k \cdots i_n) , \quad (5)$$

where $\widehat{i}_k$ means to exclude this site. Each simplex $\sigma_n(i_0 i_1 \cdots i_n)$ is an anti-symmetric function of its arguments. The signs in Eq. (5) keep track of the orientation of each simplex. It is trivial to check that the boundary operator is closed: $\partial^2 \sigma_n = 0$. On a finite simplicial lattice ∂ is a matrix and its transpose, ∂^T, is the co-boundary operator. This is a first modest step into discrete homology and De Rham cohomology on a simplicial complex.

In the next layer, Regge Calculus introduces a metric by assigning lengths to the edges $l_{ij} = |\sigma_1(ij)|$, which provides the discrete metric, $g \to g_\sigma$, assuming the interior of each D-plex is a flat Euclidean space (e.g., piecewise linear coordinates). This lifts the simplex into a metric space. For example, oriented links, $\langle i, j \rangle = \sigma_1(ij)$, are now associated with vectors, $\vec{l}_{ij}$ and triangles, $\triangle_{ijk} = \sigma_2(ijk)$, with areas A_{ijk} and so on. Since the cells are flat, the curvature tensor required for Einstein gravity in Regge Calculus has singularities on the boundary, i.e., at vertices in 2D and hinges for $D > 2$. Matter fields (or forms) are nth-rank tensors, naturally assigned to σ_n.

Next, it is important to add to our simplicial Delaunay lattice, $\mathcal{S}$, the circumcenter dual Voronoi lattice, $\mathcal{S}^*$,

composed of polytopes, $\sigma_0^* \leftarrow \sigma_1^* \leftarrow \cdots \leftarrow \sigma_D^*$ where σ_n^* has dimension $D - n$ as illustrated in Fig. 1. A crucial property of this circumcenter duality is **orthogonality**. Each simplicial element $\sigma_n \in S$ is orthogonal to its dual polytope $\sigma_n^* \in S^*$. This orthogonality lies at the heart of defining the Hodge star $*$ (or alternating symbol $\epsilon^{i_0 i_1 \cdots i_D}$). The circumcenters for the dual lattice can be found iteratively. The circumcenter of an edge $\langle i, j \rangle = \sigma_1(ij)$ is its midpoint, the circumcenter of a triangle $\triangle_{ijk} = \sigma_2(ijk)$ lies at intersection of the perpendiculars from the midpoints of the aforementioned boundary edges $\sigma_1 \in \partial \sigma_2(ijk)$, the circumcenter of a tetrahedron σ_3 lies at the intersection of the normals from the circumcenters of its boundary triangles, etc., as we move into higher dimensions.

Hybrid cells, $\sigma_n \wedge \sigma_n^*$, constructed from simplices σ_n in $\mathcal{S}$ and their orthogonal dual σ_n^* in $\mathcal{S}^*$ give a proper tiling of the discrete manifold. As a consequence of this orthogonality, the volume $V_{nn*} = |\sigma_n \wedge \sigma_n^*|$ of the hybrid $\sigma_n \perp \sigma_n^*$ is a simple product,

$$V_{nn*} = \langle \sigma_n | \sigma_n^* \rangle = \int \sigma_n \wedge \sigma_n^* = \frac{n!(D-n)!}{D!} |\sigma_n| |\sigma_n^*| . \quad (6)$$

For future reference, we introduce a simplified notation in lower dimensions: the point, length of links, and area of triangles will be given by

$$1 = |\sigma_0(i)| \quad , \quad l_{ij} = |\sigma_1(ij)| \quad , \quad A_{ijk} = |\sigma_2(ijk)| \quad (7)$$

respectively and the D-dimensional hybrid volumes associated with sites, links and triangles will be designated by

$$V_i = |\sigma_0^*(i)| \, , \, V_{ij} = |\sigma_1(ij) \wedge \sigma_1^*(ij))|$$
$$V_{ijk} = |\sigma_2(ijk) \wedge \sigma_2^*(ijk)| , \quad (8)$$

respectively. Finally, when we add matter fields ω for scalar (ϕ_i), Dirac (ψ_i) and gauge fields (U_{ij}), we can define a discrete exterior derivative d (or finite difference for grad, div and curl) through a discrete Stokes' theorem on the simplex,

$$\int_{\sigma_n} d\omega(y) = \int_{\partial \sigma_n} \omega(y) \quad \text{or} \quad \langle \sigma_n | d\omega \rangle = \langle \partial \sigma_n | \omega \rangle . \quad (9)$$

The Hodge star takes you to the dual simplex σ_n^* to define the dual operator, $\delta = *d*$. The operators δ, d automatically inherit from ∂, ∂^T, respectively the closure property, $d^2 = \delta^2 = 0$. While we do not rely heavily on this formalism, it is useful intuitively to guide our discussion. This formal layered structure, we believe, is also important for organizing software to implement lattice field theory simulations on general simplicial lattices.
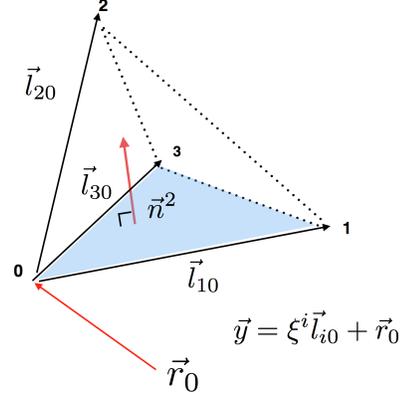
FIG. 2. The D-simplex, illustrated for $D = 3$, can be defined by D edge vectors $\vec{l}_{i0} = \vec{r}_i - \vec{r}_0$, picking arbitrarily the 0-th vertex. The remaining $D(D-1)/2$ edges are $\vec{l}_{ij} = \vec{l}_{i0} - \vec{l}_{j0}$. One dual vector $\vec{n}^2$ normal to $\sigma_2(013)$ is depicted.

B. Simplicial Laplacian for Scalar Fields

The flat interior of each D-simplex in RC and FEM is conveniently parameterized as

$$\vec{y} = \xi^0 \vec{r}_0 + \xi^1 \vec{r}_1 + \cdots + \xi^D \vec{r}_D = \sum_{i=1}^{D} \xi^i \vec{l}_{i0} + \vec{r}_0 , \quad (10)$$

using barycentric coordinates, $0 \leq \xi^i \leq 1$, with the constraint $\xi^0 + \xi^1 + \cdots + \xi^D = 1$. The vectors on the edges are $\vec{l}_{i0} = \vec{r}_i - \vec{r}_0$. To pick a unique coordinate system on $\mathcal{M}_\sigma$, we can arbitrarily eliminate ξ^0, introducing the differentials,

$$d\vec{y} = \frac{\partial \vec{y}}{\partial \xi^i} d\xi^i = \vec{l}_{i0} d\xi^i , \quad (11)$$

where $\vec{l}_{i0}$ are the components of this one form in the basis $d\xi^i$ with $i = 1, \cdots, D$ and dual tangent vectors,

$$\vec{\nabla} = \vec{\nabla} \xi^i \partial_i = \vec{n}^i \partial_i , \quad (12)$$

with components, $\vec{n}^i = \nabla \xi^i$ in the basis ∂_i. The flat metric on each simplex is

$$ds^2 = d\vec{y} \cdot d\vec{y} = g_{ij} d\xi^i d\xi^j,$$
$$g_{ij} = \vec{l}_{i0} \cdot \vec{l}_{j0} = \frac{1}{2}(l_{i0}^2 + l_{j0}^2 - l_{ij}^2) . \quad (13)$$

The standard relations for raising and lowering indices by the metric tensor (g_{ij}) and its inverse,

$$g^{ij} = \vec{n}^i \cdot \vec{n}^j \quad \text{or} \quad \vec{n}^i \cdot \vec{l}_{j0} = \delta_j^i , \quad (14)$$

applies within each simplex. Note since the interior of the simplex is flat we choose the notation $\vec{l}_{i0}$ and $\vec{n}^i$,

$$\vec{l}_{i0} \rightarrow l_{i0}^a = \frac{\partial y^a}{\partial \xi^i} \quad \text{and} \quad \vec{n}^i \rightarrow n_a^i = \frac{\partial \xi^i}{\partial y^a} , \quad (15)$$

for both upper and lower indices. It is tempting to use the notation, $\vec{l}_{0i} \to \vec{e}_i$ and $\vec{n}^i \to \vec{e}^i = g^{ij}\vec{e}_j$, but we reserve this identification with lattice vierbeins for the simplicial Dirac equation in Secs. III and IV.

The new action on the simplicial manifold $(\mathcal{M}_\sigma, g_\sigma)$ is again determined by Eq. (1) using the simplicial metric (13). It is given by a sum over all the D-simplices,

$$S_\sigma = \frac{1}{2} \sum_{\sigma_D} \int_{\sigma_D} d^D y [\vec{\nabla}\phi_\sigma(y) \cdot \vec{\nabla}\phi_\sigma(y) + m^2\phi_\sigma^2(y)] \quad (16)$$

$$= \frac{1}{2} \sum_{\sigma_D} \int_{\sigma_D} d^D\xi \sqrt{g_\sigma}\, [g_\sigma^{ij}\partial_i\phi_\sigma(\xi)\partial_j\phi_\sigma(\xi) + m^2\phi_\sigma^2(\xi)] ,$$

where $\sqrt{g_\sigma}/D! = |\sigma_D|$ is the volume in each D-simplex, or in 2D the area A_{ijk} of the triangle $\triangle_{ijk}$. Finally, we expand $\phi_\sigma(y)$ in a finite element basis on **each** simplex,

$$\phi_\sigma(y) \simeq E^0(y)\phi_0 + E^1(y)\phi_1 + \cdots + E^D(y)\phi_D , \quad (17)$$

where $E^i(r_j) = \delta^i_j$ so that $\phi_i = \phi(y = r_i)$. We also impose the sum rule, $\sum_i E^i(y) = 1$, so that the constant field is preserved. **For simplicity, our subscript on ϕ_σ, S_σ, etc, implies a restriction to a single simplex, $\sigma_D(i_0 i_1 \cdots i_D)$.** The expansion of the field over the entire piecewise flat manifold, $(\mathcal{M}_\sigma, g_\sigma)$, is given by a sum over all sites, $\phi(x) \simeq \sum_i W^i(y)\phi_i$, where the $W^i(y)$'s , referred to as *tent functions* , are sums over all adjacent elements, $E^i(y)$'s, that have non-zero (unit) support at the site i. Once these elements $E^i(y)$ are chosen, explicit integration for the simplicial action, Eq. (17), can be carried out, leading to a quadratic form for the free field action on the values ϕ_i. This construction also carries over for interaction terms, $\phi^n(x)$, giving higher order polynomials in ϕ_i within each simplex.

The simplest choice is the *linear FEM*,

$$E^i(\xi) = \xi^i, \qquad i = 0, \cdots D . \quad (18)$$

Since all the derivatives are constants, the massless action on each simplex,

$$I_\sigma = \frac{1}{2} \int_{\sigma_D} d^D y \vec{\nabla}\phi(y) \cdot \vec{\nabla}\phi(y)$$

$$= \frac{1}{2} \int_{\sigma_D} d^D\xi \sqrt{g} g^{ij}\partial_i\phi(\xi)\partial_j\phi(\xi), \quad (19)$$

is trivially evaluated, giving

$$I_\sigma = \frac{1}{2D!} \sum_{i,j=1}^{D} \sqrt{g}\, g^{ij}(\phi_i - \phi_0)(\phi_j - \phi_0) . \quad (20)$$

While this result (20) is correct, one inconvenience is that our arbitrary choice of eliminating ξ^0 appears to break the symmetry between the $D + 1$ sites. To fix this we may average over the $D + 1$ vertices to yield the correct symmetrized expression, which will be referred to as the **Vertex Form** (illustrated for $D = 2$ in Fig. 3) of the simplicial action.
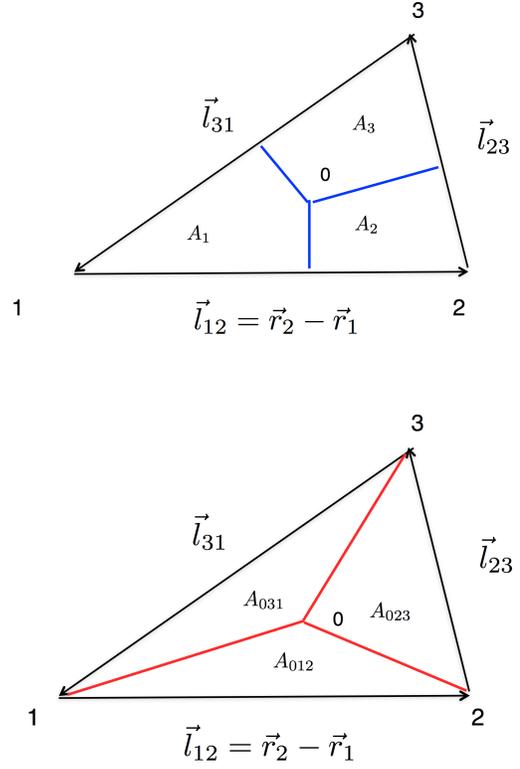
FIG. 3. The geometric contribution of linear finite elements to a scalar field in the **Vertex form** in the top figure and in the **Link form** in the bottom figure. For both forms, the triangle $\triangle_{123}$ is subdivided into regions meeting at the circumcenter 0, with areas $A_i = |\sigma^*(i) \cap \triangle_{123}|$ and $A_{0ij} = |\sigma_1(ij) \wedge \sigma_1^*(ij) \cap \triangle_{123}|$, respectively.

However, a more appealing geometric form can be found. A convenient way to derive this is to relax the constraint $\xi_0 + \cdots + \xi_D = 1$ and introduce an over complete set of $D + 1$ dual vectors, $\vec{n}^k = \vec{\nabla}\xi^k$, that are perpendicular to the face opposite the vertex k and normalized relative to the edge vectors by

$$\vec{n}^k \cdot \vec{l}_{ij} = \delta^k_i - \delta^k_j . \quad (21)$$

In this over-complete basis , the gradient is $\vec{\nabla}\phi(y) = \vec{n}^0\phi_0 + \vec{n}^1\phi_1 + \cdots + \vec{n}^D\phi_D$. Evaluating the action gives two equivalent symmetric forms,

$$I_\sigma = \frac{1}{2} \sum_{i,j=0}^{D} |\sigma_D|\, \vec{n}^i \cdot \vec{n}^j \phi_i\phi_j$$

$$= \frac{1}{2} \sum_{\langle i,j \rangle} |\sigma_D|\, (-\vec{n}^i \cdot \vec{n}^j)(\phi_i - \phi_j)^2 , \quad (22)$$

due to the constraint,

$$\vec{\nabla}(\xi^0 + \xi^1 + \cdots + \xi^D) = \vec{n}^0 + \vec{n}^1 + \cdots + \vec{n}^D = 0 . \quad (23)$$

Recall that $|\sigma_D| = \sqrt{g_\sigma}|/D!$ is the volume of D-simplex. We refer to this as the **Link Form** (illustrated for $D = 2$ in Fig. 3). In two dimensions summing over all the triangles, the contribution to the lattice action takes an appealing geometric form

$$S_\sigma = \frac{1}{2} \sum_{\langle i,j \rangle} A_{ij} \frac{(\phi_i - \phi_j)^2}{l_{ij}^2} \, , \qquad (24)$$

where in 2D we use the notation $A_{ij} = |\sigma_1(ij) \wedge \sigma_1^*(ij)|$, instead of V_{ij}, for the dual area Eq. (6) adjacent to the link $\langle i,j \rangle$.

Discrete Exterior Calculus: An alternative formalism for constructing the simplicial Laplacian relies on an elegant Discrete Exterior Calculus (DEC) [9]. For any dimension, the DEC action for the kinetic term is given by

$$S_\sigma[\phi] = \frac{1}{2} \sum_{\langle i,j \rangle} V_{ij} \frac{(\phi_i - \phi_j)^2}{l_{ij}^2} + \frac{1}{2} m^2 V_i \phi_i^2 \, , \qquad (25)$$

where, as illustrated in Fig. 4 in 2D, $V_{ij} = |\sigma_1(ij) \wedge \sigma_1^*(ij)| = l_{ij} S_{ij}/D$ is the product of the length of the link (l_{ij}) times the volume of the surface, $S_{ij} = |\sigma_1^*(ij)|$, of the dual polytope normal to the link $\langle i,j \rangle$. A local mass term has been added for future reference even though it does not contribute to the Laplacian. **Only in 2D is the linear FEM form (22) equivalent to the DEC form (25).** In 2D the equivalence follows from the identity, $A_{123} \vec{n}_1 \cdot \vec{n}_2 = A_{ij}/l_{12}^2$, often referred to as the co-tangent rule. But for $D > 2$, it is easy show how this fails by constructing a a counter example: Pick a simplex for $D > 2$ with $\vec{n}_1 \cdot \vec{n}_2 = 0$ and $V_{ij} > 0$ that vanish for the linear FEM construction but in non-zero for the DEC construction.

The DEC construction for the discrete Beltrami-Laplace operator,

$$\frac{1}{V_i} \frac{\partial S_\sigma[\phi]}{\partial \phi_i} = \frac{1}{V_i} \sum_{j \in \langle i,j \rangle} \frac{V_{ij}}{l_{ij}} \frac{\phi_i - \phi_j}{l_{ij}} \, , \qquad (26)$$

follows the same basic steps leading to the continuum operator $-\frac{1}{\sqrt{g}} \partial_\mu \sqrt{g} g^{\mu\nu} \partial_\nu \phi(x)$. First, we apply the simplicial Stokes' theorem, Eq. (9), to get the discrete gradient (exterior derivative),

$$d\phi = \frac{1}{|\sigma_1(ij)|} \int_{\sigma_1} d\phi(x) = \int_{\partial\sigma_1} \frac{\phi(x)}{l_{ij}} = \frac{\phi_i - \phi_j}{l_{ij}} \, , \quad (27)$$

where the scalar (or zero form) ϕ_i and the finite difference (or one form), $d\phi_i = (\phi_i - \phi_j)/l_{ij}$, are assigned to sites $\sigma_0(i)$ and links $\sigma_1(ij)$ respectively. Next, apply Stokes' theorem again on the dual lattice polytope σ_0^* to compute the divergence, $d(*d\phi_i)$, illustrated in yellow in Fig. 4 for 2D and return to the simplicial lattice,

$$*d*d\phi_i = * \frac{1}{|\sigma_0^*(i)|} \int_{\sigma_0^*} d[*(\phi_i - \phi_j)/l_{ij}]$$

$$= \frac{1}{V_i} \sum_{j \in \langle i,j \rangle} \frac{V_{ij}}{l_{ij}} \frac{\phi_i - \phi_j}{l_{ij}} \, , \qquad (28)$$
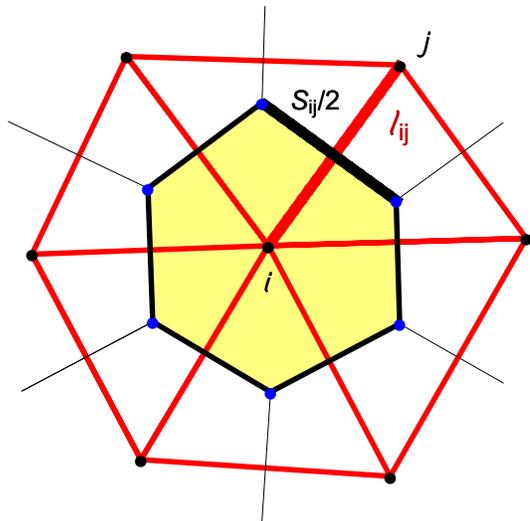
FIG. 4. The discrete Laplacian at a site i is given by the sum on all links $\langle i,j \rangle$ (in red) weighed by gradients $(\phi_i - \phi_j)/l_{ij}$ multiplied by the surface $S_{ij} = 2V_{ij}/l_{ij}$ (in black) and normalized by the dual volume $|\sigma_o^*(i)| = V_i$ (in yellow).

in agreement with Eq. (26), expressed as the sum of fluxes through the boundaries $\partial\sigma_0^*(i)$ with surface area, $S_{ij}/(D-1)! = V_{ij}/l_{ij} = |\sigma_1(ij) \wedge \sigma_1^*(ij)|/l_{ij}$. For the local mass term one would add $m \int_{\sigma_0^*} \phi_i/|\sigma_0^*| = m^2 \phi_i$ to the operator (28).

III. DIRAC FIELDS ON A RIEMANN MANIFOLD

The action of the free Dirac fermion on a Riemann manifold,

$$S = \int d^D x \sqrt{g} \bar\psi(x) [\mathbf{e}^\mu(x)(\partial_\mu - i\boldsymbol{\omega}_\mu(x)) + m]\psi(x) \, , \ (29)$$

introduces two new structures involving spin: (i) The orientation of the spinor in the tangent plane, $\mathbf{e}^\mu(x) = e_a^\mu(x)\gamma^a$, where e_a^ν is the inverse (or dual) of the vierbein, e_μ^a, entering into the metric. (ii) The spin connection $\boldsymbol{\omega}_\mu(x) \equiv \omega_\mu^{ab}(x)\sigma_{ab}/4$, where $\sigma_{ab}/2 = i[\gamma_a, \gamma_b]/4$ are the Lorentz generators for the Dirac spinor. The reason for this is because there are no finite-dimensional spinor representations of the general covariance group, so spinor indices are introduced in the tangent space. At each point x^μ, the flat tangent space can be spanned by a set of orthonormal coordinates, $\vec{y} = (y^1(x), y^2(x), \cdots, y^D(x))$, by expanding the cotangent differential,

$$dy^a = e_\mu^a(x)dx^\mu = \frac{\partial y^a}{\partial x^\mu} dx^\mu \, . \qquad (30)$$

The positive definite metric,

$$ds^2 = d\vec{y} \cdot d\vec{y} = e_\mu^a(x)e_\nu^a(x)dx^\mu dx^\nu = g_{\mu\nu}dx^\mu dx^\nu \, , \ (31)$$

can be Cholesky factorized in terms of $e_\mu^a(x)$. Now in addition to invariance under diffeomorphism, there is a local "gauge" invariance allowing an arbitrary rotation (or Euclidean Lorentz transformation), $SO(D)$, in the tangent plane: $y^a \to O_b^a y^b$. This then acts on the spinors as a gauge invariance in the $\texttt{Spin}(D)$ covering group.

The spin connection and the vierbeins are not independent. For torsion-free and metric compatible Riemann manifolds, they are related through the tetrad hypothesis,

$$\partial_\mu \boldsymbol{e}^\nu(x) + \Gamma_{\mu\lambda}^\nu \boldsymbol{e}^\lambda = i[\boldsymbol{\omega}_\mu, \boldsymbol{e}^\nu] , \tag{32}$$

or $[\boldsymbol{D}_\mu, \boldsymbol{e}^\nu] + \Gamma_{\mu\lambda}^\nu \boldsymbol{e}^\lambda = 0$, where $\boldsymbol{D}_\mu = \partial_\mu - i\boldsymbol{\omega}_\mu$ is the "covariant spinor derivative" operator. Expanding in components we have

$$\omega_\mu^{ab} = e_\nu^a \partial_\mu e_b^\nu + e_\lambda^a \Gamma_{\mu\nu}^\lambda e_b^\nu$$
$$= \frac{1}{2} e_a^\nu [\partial_\mu e_\nu^b - \partial_\nu e_\mu^b + e_b^\rho e_\mu^c \partial_\nu e_\rho^c] - (a \leftrightarrow b) . \tag{33}$$

A crucial consequence of the tetrad hypothesis (32) is the anti-Hermitian property of Dirac operator,

$$(\sqrt{g}\mathbf{e}^\mu \boldsymbol{D}_\mu)^\dagger = -\boldsymbol{D}_\mu \sqrt{g}\mathbf{e}^\mu$$
$$= -\sqrt{g}(\mathbf{e}^\mu \boldsymbol{D}_\mu + [\boldsymbol{D}_\mu, \mathbf{e}^\mu] + \frac{1}{\sqrt{g}}(\partial_\mu \sqrt{g})\mathbf{e}^\mu)$$
$$= -\sqrt{g}\mathbf{e}^\mu \boldsymbol{D}_\mu . \tag{34}$$

Consequently the Dirac spectrum on a general manifold is pure imaginary plus the real mass shift: $i\lambda + m$ with $-\infty < \lambda < \infty$. It is essential when placing the Dirac equation on a simplicial manifold to provide a lattice realization for this identity.

A. The Dirac Finite Element

The application of classical FEM methods to fermions leads to a series of difficulties. First, even in 2D, linear finite elements in flat space do not give a natural generalization of the scalar FEM expression. Second, the well-known problem of species doubling and chiral symmetry breaking is not solved by a straight forward application of FEM. Third, and most troubling, in the Regge Calculus representation of a linear simplicial manifold, the curvature has singularities concentrated at the vertices and hinges. It is difficult, if not impossible, to place Dirac fields at such singular vertices as there is no well-defined tangent plane. We proceed to address the solution to these difficulties one by one.

A reasonable ansatz for a simplicial fermion in flat space is a generalization of the DEC scalar form in Eq. (25),

$$S_{naive} \simeq \frac{1}{2} \frac{V_{ij}}{l_{ij}^2} [\bar{\psi}_i \vec{l}_{ij} \cdot \vec{\gamma} \psi_j - \bar{\psi}_j \vec{l}_{ij} \cdot \vec{\gamma} \psi_i] + \frac{1}{2} m V_i \bar{\psi}_i \psi_i , \tag{35}$$

also recommend by Friedberg, T.D. Lee, and Ren in Ref. [15]. We shall refer to this as the **canonical Dirac**
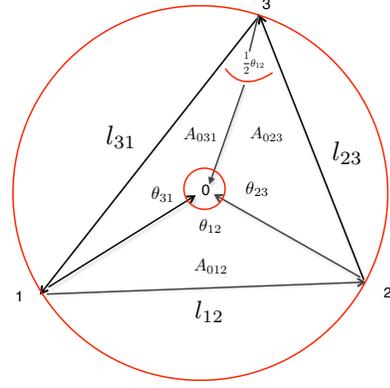
FIG. 5. A new Dirac finite element on the simplex splits the each triangle, $\triangle_{123}$, with edge vectors $(\vec{l}_{12}, \vec{l}_{23}, \vec{l}_{31})$ into three isosceles sub-triangles that meet at the dual vertex 0. An interior angle at 0 opposite a link $\vec{l}_{ij}$ is designated as θ_{ij}.

form. However, this form is **not** given by the application of linear FEM to the Dirac field.

Following closely the scalar example (22), the linear FEM evaluation of the Dirac action on each simplex is

$$\int_\sigma d^D y[\psi(y)\vec{\gamma}\cdot\vec{\nabla}\psi(y) = \frac{\sqrt{g}}{2(D+1)!} \sum_i \psi_i \; \vec{n}^{\;j}\cdot\vec{\gamma}\psi_j . \tag{36}$$

For anti-Hermiticity to be enforced, one must explicitly sum over the oriented and anti-oriented simplex, resulting in

$$I_\sigma = \frac{1}{2} \int_\sigma d^D y[\psi(y)\vec{\gamma}\cdot\vec{\nabla}\psi(y) - (\vec{\nabla}\psi(y))\cdot\vec{\gamma}\psi(y)] \tag{37}$$
$$= \frac{\sqrt{g}}{4(D+1)!} \sum_{\langle i,j \rangle} \bar{\psi}_i(\vec{n}^{\;j} - \vec{n}^{\;i})\cdot\vec{\gamma}\psi_j . \tag{38}$$

However, even for $D = 2$, the linear FEM formula,

$$S_\sigma = \frac{A_{123}}{6} \sum_{\langle i,j \rangle} \bar{\psi}_i(\vec{n}^{\;j} - \vec{n}^{\;i})\cdot\vec{\sigma}\psi_j , \tag{39}$$

fails to give the **canonical Dirac form**. Most peculiarly, the spin projections $\vec{l}_{ij}\cdot\vec{\sigma}$ are not aligned with the propagation on the links. Namely the condition $\vec{n}^{\;k}\cdot(\vec{n}^{\;i} - \vec{n}^{\;j}) = 0$, required by alignment, $\vec{l}_{ij} \sim \vec{n}^{\;i} - \vec{n}^{\;j}$, fails except for an equilateral triangle where the dual vectors are normal to the opposite sides. However, we have found a new **Dirac Finite Element** prescription that does lead to the canonical lattice form in 2D by summing over the piecewise linear elements for each of 3 sub-triangles meeting at the circumcenter of a general triangle as illustrated in Fig. 5.

The new construction begins by expanding $\triangle_{123}$ in a new finite element basis,

$$\psi_\sigma(y) = E^1(y)\psi_1 + E^2(y)\psi_2 + E^3(y)\psi_3 ,$$
$$\bar{\psi}_\sigma(y) = E^1(y)\bar{\psi}_1 + E^2(y)\bar{\psi}_2 + E^3(y)\bar{\psi}_3 , \tag{40}$$

imposing basic properties for field interpolates,

$$E^i(r_j) = \delta^i_j \quad , \quad E^1(y) + E^2(y) + E^3(y) = 1 , \quad (41)$$

so that $\psi(r_i) = \psi_i$ and a constant field is preserved. We then make the ansatz that the element can be decomposed into three elements meeting at the circumcenter. We introduce ghost fields, ψ_0 and $\bar\psi_0$, at the circumcenter of each triangle and expand the fields $\psi(x), \bar\psi(x)$ as the sum of 3 piecewise linear elements, one on each subtriangle. The ghost fields are expressed as a linear combination of the original lattice values,

$$\psi_0 = c_1\psi_1 + c_2\psi_2 + c_3\psi_3 ,$$
$$\bar\psi_0 = c_1\bar\psi_1 + c_2\bar\psi_2 + c_3\bar\psi_3 . \quad (42)$$

The constraint $\sum_i c_i = 1$ is required so that the constant field is preserved. This implicitly defines the new Dirac elements (40) $E^i(y)$ on the full triangle Δ_{123}. By a judicious choice of the coefficients,

$$c_k = \frac{4A_{0ij}}{l^2_{ij}} \frac{4A_{0ik}}{l^2_{ik}} = \cot(\theta_{ik}/2)\cot(\theta_{jk}/2) , \quad (43)$$

this new Dirac FEM construct leads to the **canonical Dirac form** (35), with all couplings along the edges properly aligned. (See Appendix A for a detailed proof.)

One benefit of this construction is that this should allow standard FEM convergence theorems to be applied to our Dirac FEM. However, we have not yet sought a generalization of this FEM construction to $D > 2$. Moreover, in spite of the intuitive appeal of our ansatz, there is no known generalization of the formalism of exterior calculus to a single Dirac fermion, analogous to the use of the Hodge star operator for the Laplace-Beltrami operator. The closest example is the application to Kähler-Dirac fermion [16]. This is an interesting area for future investigation [17].

B. The Simplicial Spin Connection

In preparation for curved space, we will first consider the simplicial complex for a flat manifold after, applying at each site i, an arbitrary rotation by a Lorentz transformation, $O(D)$, on the tangent vectors. The result is to transform each spinor: $\psi_i \to \Lambda_i\psi_i$, with $\Lambda_i \in \text{Spin}(D)$. The action in this general gauge becomes,

$$S_{naive} = \frac{1}{2}\sum_{\langle i,j\rangle} \frac{V_{ij}}{l_{ij}}[\bar\psi_i\vec{e}^{\,(i)j}\cdot\vec\gamma\Omega_{ij}\psi_j - \bar\psi_j\Omega_{ji}\vec{e}^{\,(i)j}\cdot\vec\gamma\psi_i]$$
$$+ \frac{1}{2}mV_i\bar\psi_i\psi_i , \quad (44)$$

where $\Omega_{ij} = \Lambda^\dagger_i\Lambda_j = \Omega^\dagger_{ji}$ serves as the lattice spin connection and $\vec{e}^{\,(i)j}$ serves as the lattice vierbein. The link variable,

$$\Omega_{ij} = e^{il^\mu_{ij}\boldsymbol{\omega}_\mu(x)} , \quad (45)$$

is entirely analogous to the compact Wilson gauge variables, $U_\mu(x) = \exp[iA_\mu(x)]$, for color spinors in lattice gauge theories: $A^{ab}_\mu(x) = \lambda^{ab}_c A^c_\mu(x)$ and $\boldsymbol{\omega}_\mu(x) = \omega^{ab}_\mu(x)\sigma_{ab}/4$ are in the Lie algebra of the color $SU(N)$ and $\text{Spin}(D)$ groups respectively. The lattice vierbein is

$$\mathbf{e}^{(i)j} = e^{(i)j}_a\gamma^a \equiv \vec{e}^{\,(i)j}\cdot\vec\gamma = \Lambda^\dagger_i\hat{l}_{ij}\cdot\vec\gamma\Lambda_i , \quad (46)$$

where $\hat{l}_{ij}$ is the out-going unit vector from i to j. With $m = 0$, the naive Dirac action is anti-Hermitian by the virtue of the identity, $\Omega_{ji}\mathbf{e}^{(i)j} = -\mathbf{e}^{(j)i}\Omega_{ji}$. Note that moving the vierbein to the opposite end of the link gives

$$e^{(j)i}_a\gamma^a = -\Omega_{ji}e^{(i)j}_a\gamma^a\Omega_{ij} , \quad (47)$$

which is the lattice realization of the tetrad hypothesis. In Sec. IV, we demonstrate that Eq. (47) is equivalent to the continuum tetrad hypothesis Eq. (32) as $l_{ij} \to 0$. Although in flat space, this spin connection is gauge equivalent to $\Omega_{ij} = 1$, we will show shortly that the parametric form of the action given by Eq. (44) now applies to any manifold with a spin connection by requiring the product of the link matrices, Ω, around a closed path to be a measure of the curvature on the triangle. Before describing the algorithm for determining a non-trivial lattice spin connection in Sec. IV, we will address the problem of species doubling.

C. The Wilson Term

At this point we have replaced the first derivative continuum operator, $\nabla = \mathbf{e}^\mu\boldsymbol{D}_\mu = \mathbf{e}^\mu(\partial_\mu - i\boldsymbol{\omega}_\mu)$, with the *naive* or central difference form on the simplex, gauged by the compact spin connections in Eq. (44). This simplicial discretization preserves the anti-Hermiticity condition of the continuum, $\nabla^\dagger\sqrt{g} = -\sqrt{g}\nabla$, and therefore it preserves the spectral property, $(\nabla + m)\psi_\lambda = (i\lambda + m)\psi_\lambda$, with $-\infty < \lambda < \infty$ as well. However, this spectrum includes spurious, or so called doubler, states familiar to the naive fermion on the hypercubic lattice. The FEM methods do not solve this problem.

To remove these doublers, we introduce a spinor gauged Wilson term in close analogy with conventional non-Abelian flat space lattice gauge field theory. The 4D lattice field theory doublers are removed by adding an irrelevant dimension 5 Wilson term to the fermions action. This discrete approximation to the continuum operator is contained in the square of the covariant Dirac operator,

$$[\gamma^\mu(\partial_\mu - iA_\mu)]^2 = (\partial_\mu - iA_\mu)^2 + \sigma_{\mu\nu}F^{\mu\nu} . \quad (48)$$

When placed on a regular lattice, the first term is referred to as the Wilson (or gauge Laplacian) term, while the second is referred to as the clover term. On a flat manifold, the doublers can be removed by adding the Wilson term. The free spectrum in momentum space of the Wilson term is proportional to $\sum_\mu(1 - \cos(ap_\mu))/a$

which is irrelevant at $p \to 0$ but divergent as $a \to 0$ for doublers on the edge of the Brillouin zone.

A similar approach can be applied to curved space. Consider adding to the action a second order derivative term,

$$\int d^D x \sqrt{g} |\nabla \psi|^2 = \int d^D x \sqrt{g} (\bar{\psi} \overleftarrow{\nabla}^\dagger)(\nabla \psi)$$
$$= -\int d^D x \sqrt{g} \bar{\psi} \nabla^2 \psi , \qquad (49)$$

using $\nabla^\dagger \sqrt{g} = -\sqrt{g} \nabla$. The square of the spinorial Dirac operator, $\nabla = \mathbf{e}^\mu \boldsymbol{D}_\mu = e^\mu_a \gamma^a \boldsymbol{D}_\mu$, is give by the Lichnerowicz formula,

$$-\nabla^2 = -g^{\mu\nu}(\boldsymbol{D}_\mu \boldsymbol{D}_\nu - \Gamma^\sigma_{\mu\nu} \boldsymbol{D}_\sigma) + \frac{1}{2}\sigma^{ab} e^\mu_a e^\nu_b \boldsymbol{R}_{\mu\nu}$$
$$= -\frac{1}{\sqrt{g}} \boldsymbol{D}_\mu \sqrt{g} g^{\mu\nu} \boldsymbol{D}_\nu + \frac{1}{2}\sigma^{ab} e^\mu_a e^\nu_b \boldsymbol{R}_{\mu\nu} . \qquad (50)$$

The first term on the second line is nothing but the covariant spinor Laplacian, while the second term is related to the curvature,

$$\boldsymbol{R}_{\mu\nu} = i[\boldsymbol{D}_\mu, \boldsymbol{D}_\nu] = i[\partial_\mu - i\boldsymbol{\omega}_\mu, \partial_\nu - i\boldsymbol{\omega}_\nu] . \qquad (51)$$

We introduce a lattice version of the covariant spinor Laplacian as a Wilson term to remove doublers on the simplicial lattice. This is just our lattice Laplace-Beltrami operator for the scalar in Eq. (26) in a general gauge,

$$S_{WilsonTerm} = \frac{r}{2} \sum_{\langle i,j \rangle} \frac{V_{ij}}{l^2_{ij}} (\bar{\psi}_i - \bar{\psi}_j \Omega_{ji})(\psi_i - \Omega_{ij}\psi_j) . \qquad (52)$$

Again, this canonical form generalizes to simplicial Dirac fermions on a general Riemann manifold. Further generalizations to include color gauge fields and to construct Domain Wall actions are straightforward as briefly mentioned in the conclusion.

IV. LATTICE SPIN STRUCTURE

We now present a procedure for fixing the vierbein $\vec{e}^{\,(i)j}$ and connection matrix, Ω_{ij}, on each link $\langle i,j \rangle$ of the simplicial lattice. Once this has been accomplished, the parametric form for a general Riemann manifold,

$$S = \frac{1}{2} \sum_{\langle i,j \rangle} \frac{V_{ij}}{l_{ij}} [\bar{\psi}_i \mathbf{e}^{(i)j} \Omega_{ij} \psi_j - \bar{\psi}_j \Omega_{ji} \mathbf{e}^{(i)j} \psi_i]$$
$$+ \frac{m}{2} \bar{\psi}_i \psi_i , \qquad (53)$$

is unchanged from the flat space formula (44). The spin connection matrices, $\Omega_{ij} = \Omega^\dagger_{ij}$, are no longer equivalent to a pure gauge transformation. A successful construction must respect the exact lattice tetrad hypothesis (47),

$$\mathbf{e}^{(i)j} \Omega_{ij} + \Omega_{ij} \mathbf{e}^{(j)i} = 0 , \qquad (54)$$
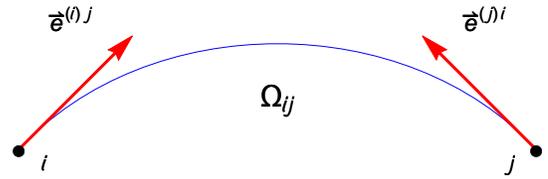
FIG. 6. The tangent vectors $\vec{e}^{\,(i)j}$ and $\vec{e}^{\,(j)i}$ on opposite sides of the geodesics on the link $\langle i,j \rangle$ are related by a parallel transport, $\mathbf{e}^{(j)i} \equiv \vec{e}^{\,(j)i} \cdot \vec{\gamma} = -\Omega_{ji} \vec{e}^{\,(i)j} \cdot \vec{\gamma} \Omega_{ij}$.

in order to ensure that the naive lattice Dirac operator, Eq. (53) is anti-Hermitian in the massless limit, or equivalently the full operator including the mass term in Eq. (53) and the Wilson term in Eq. (52) is γ_5-Hermitian. This gauge covariant identity in Eq. (54), arising from parallel transports of the vierbein along the link, is crucial to the construction. If we expand in the lattice spacing, a, we can immediately see how it is a discrete version of the continuum Eq. (32). In Fig. 6 let i and j be located at $x^\mu = x^\mu(0)$ and $x^\mu(1) = x^\mu(0) + a\hat{l}^\mu$, respectively, on the geodesic, $x^\mu(s)$, between them. Introduce a smooth bi-spinor field, $\mathbf{e}(x) = t_\nu(x)\mathbf{e}^\nu(x)$. Expanding $\mathbf{e}^{(j)i} + \Omega^\dagger_{ij}\mathbf{e}^{(i)j}\Omega_{ij}$ term by term, we get

$$0 = \hat{t}_\nu(x + a\hat{l})\mathbf{e}^\nu(x + a\hat{l})$$
$$- e^{ial^\mu \omega_\mu(x)} \hat{t}_\nu(x)\mathbf{e}^\nu(x) e^{-ial^\mu \omega_\mu(x)}$$
$$\simeq a\hat{t}_\nu \hat{l}^\mu \partial_\mu \mathbf{e}^\nu(x) + a\hat{t}_\nu \hat{l}^\mu \Gamma^\nu_{\mu\lambda}(x)\mathbf{e}^\lambda(x)$$
$$- ia\hat{t}_\nu \hat{l}^\mu [\omega_\mu(x), \mathbf{e}^\nu(x)] + O(a^2) , \qquad (55)$$

which is equivalent to the continuum expression, $(\partial_\mu + \Gamma^\nu_{\mu\lambda}(x))\mathbf{e}^\lambda(x) - i[\omega_\mu(x), \mathbf{e}^\nu(x)] = 0$, to leading order. In expanding Eq. (55), we have made use of the approximation $\hat{t}_\nu(x + a\hat{l}) - \hat{t}_\nu(x) \simeq a\hat{t}_\nu \hat{l}^\mu \Gamma^\nu_{\mu\lambda}(x)$ which follows from the geodesic equation (59).

In computing the spin connection for our target manifold, there are two crucial issues we need to address: **i.)** First defining the tangent plane for the Dirac field at each site. **ii.)** Second resolving the sign ambiguity in the map from the Lorentz group, $O(D)$, to the spinor covering group, $\mathtt{Spin}(D)$.

The first issue is the difficulty of defining tangent plane at the sites in the conventional piecewise flat Regge Calculus manifold. The RC defines the interior of each simplex to be flat so that all curvature is given by singularities on $D-2$ simplices at the boundary of the cells referred to as hinges, or vertices in 2D [18]. Since it is impossible to define tangent planes at the lattice sites of a piecewise linear manifold, previous attempts to introduce fermions in RC have generally placed the Dirac fields at the circumcenters of the dual lattice [7, 19–24]. However, this is troublesome for lattice gauge theory. With gauge fields on links, matter fields (scalar and Dirac) should be on sites to maintain local gauge covariance as described briefly in Sec. VII.

Our solution is to re-interpret the RC manifold as smooth, with well-defined tangent planes at the vertices. For example, on the sphere, we can remove the singular curvature at the sites by replacing each link $\langle i, j \rangle$ by geodesics (great circles in 2D). This allows us to define tangent planes at the vertices. More generally, as pointed out by Brewin [25], it is possible to provide a re-interpretation of the RC geometry. Given the RC data of a simplicial complex and the set of edges lengths l_{ij}, it is possible to construct a smooth interpolation of the curvature field, e.g., accurate to $O(a^2)$ in the continuum limit, in much the same spirit of higher splines in 1D or higher order FEM for matter fields in a general dimension. This redefinition of the Regge manifold will be implemented to fix the lattice vierbein and spin connection, however, to $O(a^2)$ we can still use the piecewise linear manifold to compute the pre-factors.

The second issue is determining the spin connection between the tangent planes on opposite ends of a link. Under parallel transport, one can compute the rotation O_{ij}, an element in the Euclidean Lorentz group $O(D)$. However we must also resolve the sign ambiguity to lift this to the spinor matrix connection, Ω_{ij}, in the $\mathtt{Spin}(D)$ group, which is the double covering of $O(D)$. The mapping,

$$O_{ij} \implies \pm \Omega_{ij} \,, \tag{56}$$

has a sign ambiguity—rotating a Dirac field by 2π changes its sign. The parallel transport of the tangent planes on a link $\langle i, j \rangle$ fixes the $O(D)$ rotation matrix O_{ij} but not the sign in the map as can be illustrated for the tetrad hypothesis, Eq. (47),

$$e_a^{(i)j}\gamma^a = -\Omega_{ij}e_a^{(j)i}\gamma^a\Omega_{ji} \implies \vec{e}^{\,(i)j} = -O_{ij}\vec{e}^{\,(j)i} \,. \tag{57}$$

The sign of the mapping in Eq. (56) onto $\mathtt{Spin}(D)$ must be fixed so that as the simplices are refined the integrated curvature on every triangle $\triangle_{123}$ vanishes in the continuum limit,

$$\Omega_{12}\Omega_{23}\Omega_{31} \simeq 1 - O(A_{123}) \to 1 \,, \tag{58}$$

and we approach the continuum Dirac equation on the Riemann manifold. This global constraint can be satisfied on a simplicial complex only if the topology of the target manifold admits a spin structure. We present here two approaches to constructing the lattice spin connection.

A. Construction by Parallel Transport

The first approach assumes that, given the continuum metric $g_{\mu\nu}(x)$, we have computed the geodesics between sites connected by links. The construction follows 3 steps:

1. Choose a random tangent frame at i and determine the tangent vectors $\vec{e}^{\,(i)j}$ on geodesics to all the neighbors at j.

2. Parallel transport the tangent frame at i to j and compute the Lorentz O_{ij}^{ab} rotation in $O(D)$ to the frame of j.

3. Map each Lorentz rotation in $O(D)$ to a pair in $\mathtt{Spin}(D)$, $O_{ij} \to s_{ij}\Omega_{ij}^{(+)}$, and choose $s_{ij} = \pm 1$, leading to the minimal curvature on each fundamental triangle.

Let us next expand on each of these steps. Consider a given link $\langle i, j \rangle$ illustrated in Fig. 6. Each site has its own tangent plane. We choose an orthonormal set of tangent vectors $\hat{t}^{\,a}(i)$ in the tangent plane given by $\vec{y} = y_a\hat{t}^{\,a}(i)$. We assume that the simplicial lattice is refined to the point that there is a unique geodesic connecting i with j. At each site i, determine the outgoing unit tangent vector $\vec{e}^{\,(i)j} \equiv e_a^{(i)j}\hat{t}^{\,a}$ aligned with the geodesic from i to j. Constructing the geodesic and the tangent vector to the geodesic requires in general numerical integration of the geodesic equation,

$$\frac{d^2x^\lambda}{ds^2} + \Gamma^\lambda_{\mu\nu}(x)\frac{dx^\mu}{ds}\frac{dx^\nu}{ds} = 0. \tag{59}$$

This gives the geodesic curve $x(s)$ from $x(0) = x_i$ to $x(s_j) = x_j$ with tangent vectors $\vec{e}^{\,(i)j} = d\vec{x}(0)/ds$ and $\vec{e}^{\,(j)i} = -d\vec{x}(s_j)/ds$ at each end.

The next step is to perform a parallel transport from the frame i to the frame j and determine the rotation between these two tangent frames: $\hat{t}^{\,a}(i) = O_{ij}^{ab}\,\hat{t}^{\,b}(j)$. The rotation for the gauge link is given by ordered product on the geodesics from i to j,

$$O_{ij} = \mathcal{P}[e^{-\int_0^{s_j} ds\,\dot{x}^\mu(s)\Gamma_\mu(x(s))}] \,, \tag{60}$$

where $[\Gamma_\mu(x(s))]^{ab} = \Gamma_\mu^{ab}(x)$ is the matrix in the Lie algebra for $O(D)$ as given in Eq (3) of [19]. This guarantees the discrete tetrad constraint (57). For simple manifolds, such as those of particular interest of conformal field theory, the exact solution to all geodesics can be determined by symmetries, avoiding numerical integration altogether. For example, on a sphere $\mathbb{S}^n$, all geodesics are defined by great circles.

Finally, for each link $\langle ij \rangle$, given $O_{ij} = e^{i\theta_{\mu\nu}J^{\mu\nu}}$, $-\pi < \theta_{\mu\nu} < \pi$, the last step involves fixing the sign ambiguity of the corresponding element Ω_{ij} in the spinor group,

$$\Omega_{ij} = s_{ij}\Omega_{ij}^{(+)}, \tag{61}$$

where $s_{ij} = \pm 1$ and $\Omega_{ij}^{(+)} = e^{i\theta_{\mu\nu}\sigma^{\mu\nu}/2} \in \mathtt{Spin}(D)$. To provide an algorithm to fix the signs on each link, we start by considering a 2D manifold. We begin by picking a random triangle and fix all s_{ij} to minimize the curvature. Then select an adjacent triangle that shares a site $\sigma_0(i)$ and one edge $\langle i, j \rangle$ with the first triangle. There are now two new links whose signs we again fix to minimize its curvature. We continue with all the triangles sharing this site i. This completes all triangles whose circumcenters make up the dual cell $\sigma^*(i)$. Now pick a new site

on the boundary of this cluster and continue. This algorithm gradually expands the closed contour around the polytopes of the dual 2D complex $\mathbb{S}^*$. As we will show explicitly for $\mathbb{S}^2$ in Sec. IV C, this continues until the last triangle which has no signs undetermined.

A failure at the last step means that the manifold does not admit a spin connection, for example, non-orientable surfaces in 2D without boundaries. The existence of a spin-structure only depends on the topology of the manifold. For example, a sphere has a trivial first homotopy group, $\pi_1(\mathbb{S}^2) = 0$, and it admits a unique spin connection. The torus has $\pi_1(\mathbb{T}^2) = \mathbb{Z}_2^2$, with 4 possible spin connections, familiar to string theorists, as Neveu-Schwarz/Neveu-Schwarz, Neveu-Schwarz/Ramond, Ramond/Neveu-Schwarz and Ramond/Ramond sectors respectively. Assume that one of the allowed multiple spin connections on the manifold is achieved. For each non-contractible loop in the dual lattice, one can introduce appropriate signs on links to exchange periodic and anti-periodic boundary conditions. This then allows one to introduce other inequivalent spin connections. More generally, a compact 2D Riemann surface of genus g admits 2^{2g} inequivalent spin structures.

This procedure can be generalized to higher dimensions along similar lines. For example, in 3D, we have an expanding closed surface. Start with a single tetrahedron and fix the signs for all edges. Then proceed to pick an edge $\sigma_1(ij)$ and visit cyclically all the tetrahedrons with circumcenters for $\sigma_1^*(ij)$ that share this edge. Now there is surface σ_{ij}^* dual to this edge $\sigma_1(ij)$. Again proceed to select a new edge on a tetrahedron on the boundary and continue as before. The 3D classification concerns the second homotopy group and 4D the third homotopy group, etc. Non-trivial homotopy groups give non-contractable surfaces with co-dimensions $D-1$ allowing one to introduce anti-periodic boundaries for multiple spin connections.

Determining the Z_2 phases, s_{ij}, only depends on the topology. For an orientable manifold in the continuum the topological condition for the existence of a spin structure is equivalent to the a vanishing of second Stiefel-Whitney class index [26]. On our lattice it is equivalent to finding the ground state in a frustrated Z_2 gauge theory. The map for $O(D)$ curvature on each triangle to $\texttt{Spin}(D)$ results in discrete Z_2 gauge theory. We must find a solution to

$$K_{ijk}\, s_{ij}s_{jk}s_{ki} = 1 \ , \tag{62}$$

where $K_{ijk} = \mathrm{Sign}[\mathrm{Tr}(\Omega_{ij}^{(+)}\Omega_{jk}^{(+)}\Omega_{ki}^{(+)})] = \pm 1$. This is equivalent to the existence of an $E = 0$ ground state for

$$E[s] = \sum_{\triangle_{ijk}} (1 - K_{ijk}\, s_{ij}s_{jk}s_{ki}) \ , \tag{63}$$

on the simplicial complex. The number of distinct ground states, mod a Z_2 local gauge invariance, enumerate inequivalent spinor representations.

B. Construction by Relaxation

Although the algorithm above is straight forward, it is computationally difficult, requiring the determination of the geodesic between neighboring lattice points and performing parallel transports of the frames to compute the rotations O_{ij}. What is needed in general is an alternative algorithm that converges to $O(a^2)$. One approach is to compare the lattice and continuum spin connections at each site of the simplicial lattice and minimize a functional to make them match up to $O(a^2)$.

The idea is to consider the lattice spin connections,

$$\Omega_{ij}^{\alpha\beta} = \big[e^{\frac{i}{2}\omega_{ab}\sigma^{ab}}\big]^{\alpha\beta} \quad \text{with} \quad \sigma^{ab} = \frac{i}{2}[\gamma^a, \gamma^b] \ , \tag{64}$$

as independent variables, choosing them to approximate as well as possible the curvature on the target manifold defined by the metric $g_{\mu\nu}(x)$. As is well known in lattice gauge theory, the product of gauge links around a "plaquette" (a triangle in this case) is an approximation to the integrated curvature over the surface. On the simplicial Regge manifold, we match the discrete curvature and the continuum curvature,

$$\Omega_{\triangle_{ijk}}^{\alpha\beta}(i) = [\Omega_{ij}\Omega_{jk}\Omega_{ki}]^{\alpha\beta}$$
$$\leftrightarrow \quad S^{\alpha\beta}(i) = \big[e^{i\boldsymbol{R}_{\mu\nu}(i)A_{\triangle_{ijk}}^{\mu\nu}}\big]^{\alpha\beta} \ , \tag{65}$$

respectively for each triangle with a vertex at a site i. The lattice estimate is just the open Wilson product on $\triangle_{ijk}(i)$ beginning and ending at a site i and the continuum estimate is the exponentiation of the local spinor curvature tensor, $\boldsymbol{R}_{\mu\nu}(i)$ in Eq. (51), projected onto the triangle. To do this, we need an estimate for the oriented area of the adjacent triangle which in the case of an isometric embedding in higher dimensions is given by

$$A_{\triangle_{ijk}}^{\mu\nu} = \frac{1}{2}[(r_i^\mu - r_j^\mu)(r_k^\nu - r_i^\nu) - (r_i^\nu - r_j^\nu)(r_k^\mu - r_i^\mu)] \ , \tag{66}$$

to $O(a^2)$. Consequently we can in principle determine the lattice spin connection by a typical relaxation algorithm, minimizing a quadratic form such as

$$G(\Omega_{ij}) = \sum_{\triangle,i} Tr[(S_\triangle(i) - \Omega_\triangle(i))^\dagger (S_\triangle(i) - \Omega_\triangle(i))] , \tag{67}$$

with respect to the unitary matrices, Ω_{ij}, in $\texttt{Spin}(D)$ on each link $\langle i, j\rangle$. The sum is over all triangles incident on each vertex i. While this prescription is not unique, any choice that is gauge invariant and converges to $O(a^2)$ in the continuum limit is acceptable. Again multiple spin connections can be generated by studying the homotopy of the simplicial complex.

Lastly, given the gauge matrices, Ω_{ij}, we also need to construct the tangent vectors $\vec{e}^{\,(i)j}$ from site i to j, consistent with the discrete tetrad hypothesis constraint, Eq. (57). It is important to focus on the fact that $\vec{e}^{\,(i)j}$ and $\vec{e}^{\,(j)i}$ are now evaluated in two different frames,

$$e_a^{(i)j}\gamma^a = -\Omega_{ij}e_a^{(j)i}\gamma^a\Omega_{ji} \ , \tag{68}$$

or $\vec{e}^{\,(i)j} = -O_{ij}\vec{e}^{\,(j)i}$. Let us first consider tangent vectors $\vec{e}^{\,(i)j}$ at i on the geodesics, $x(s)$, from i to all neighboring sites j, i.e., $x(0) = x_i$ and $x_j = x(s_j)$ at ends of the $\langle i,j \rangle$ link with s_j the geodesic length. The geodesic equation, Eq. (59), in **the same local coordinate system used to compute the curvature $R_{\mu\nu}(i)$ at site** i, determines the geodesic to $x_j(s)$ from i to each of the neighbors, j. The velocities at i are proportional to the vierbein: $\dot{x}_j(0) = dx_j/ds|_{s=0} \sim e^{\,(i)j}$.

To approximate these velocities, $\dot{x}_j(0)$, we consider a Taylor expansion [27] about $s = 0$,

$$x_j(s) = x_j(0) + s\dot{x}_j(0) + \sum_{n=2}^{\infty} \frac{s^n}{n!} \frac{d^n x_j}{ds^n}|_{s=0} , \qquad (69)$$

for the geodesic. Then using the geodesic equation (59), the nth derivative in the sum may be re-expressed as an nth order polynomial in $s\dot{x}(0)$. After substituting the rescaled velocity $v^\lambda = s_j\dot{x}_j^\lambda(0)$, the series expansion takes the form,

$$v^\lambda \simeq \Delta x_{ij}^\lambda + \sum_{n=2}^{\infty} \frac{1}{n!} \widetilde{\Gamma}^\lambda_{\mu_1,\mu_2,..,\mu_n}[x(0)] v^{\mu_1} v^{\mu_2} \cdots v^{\mu_n} , \quad (70)$$

where have brought the linear term, v^λ, and the difference, $\Delta x_{ij} = x_j(s_j) - x_j(0)$, to the left and right hand side of Eq. (70), respectively. The nth tensor coefficients $\widetilde{\Gamma}^\lambda_{\mu_1,\mu_2,..,\mu_n}[x(0)]$ are defined [27] recursively in terms of derivatives of $\Gamma^\lambda_{\mu\nu}$ and products of lower rank tensors starting with $\widetilde{\Gamma}^\lambda_{\mu\nu}[x(0)] = \Gamma^\lambda_{\mu\nu}[x(0)]$.

This simple maneuver allows us to approximate the tangent vector as a series in $\Delta x_{ij} = O(a)$ in the continuum limit. In leading order, we see that $v(0) \simeq \Delta x_{ij}$, corresponding to the fact that, on a smooth manifold, the straight line is the first approximation. The next step is to use this linear approximation in the second order equation to get a quadratic approximation. In general the nth approximation takes the form of an nth order polynomial in Δx_{ij} as described in Ref. [27], leading to

$$v^\lambda = s_j \dot{x}^\lambda(0) \simeq \Delta x_{ij}^\lambda + \frac{1}{2}\Gamma^\lambda_{\mu\nu}[x(0)]\Delta x_{ij}^\mu \Delta x_{ij}^\nu$$
$$+ C^\lambda_{\mu_1\mu_2\mu_3}\Delta x_{ij}^{\mu_1} \Delta x_{ij}^{\mu_2} \Delta x_{ij}^{\mu_3} + \cdots . \quad (71)$$

The quadratic approximation in Δx_{ij} gives $O(a^2)$ errors for the normalized tangent vector, which is sufficient for our construction.

After normalizing the velocities, we have an approximation to the lattice vierbein $E^{(i)j} \simeq \dot{x}(0)/\dot{x}(0)| \simeq e^{(i)j}$. If we repeat this construction at all sites, adopting coordinate systems at i and j sites, related by Ω_{ij}, we have an approximate solution to the lattice tetrad hypothesis: $\vec{E}^{\,(i)j} + O_{ij}\vec{E}^{\,(j)i} = O(a^2)$ on each link. Remarkably from, this approximation we can construct an exact solution to the tetrad hypothesis simply by averaging the estimate for $\vec{E}^{\,(i)j}$ at i with the pullback $(-O_{ij}\vec{E}^{\,(j)i})$

from j,

$$\vec{e}^{\,(i)j} = \frac{\vec{E}^{\,(i)j} - O_{ij}\vec{E}^{\,(j)i}}{|\vec{E}^{\,(i)j} - O_{ij}\vec{E}^{\,(j)i}|}$$
$$\vec{e}^{\,(j)i} = \frac{\vec{E}^{\,(j)i} - O_{ji}\vec{E}^{\,(i)j}}{|\vec{E}^{\,(j)i} - O_{ji}\vec{E}^{\,(i)j}|} , \qquad (72)$$

normalized to unit length. The denominators in Eq. (72) are equal, so dropping them we can verify the tetrad hypothesis identity on each link $\langle i,j \rangle$ by

$$\vec{e}^{\,(i)j} + O_{ij}\vec{e}^{\,(j)i} \qquad\qquad (73)$$
$$\sim \vec{E}^{\,(i)j} - O_{ij}\vec{E}^{\,(j)i} + O_{ij}(\vec{E}^{\,(j)i} - O_{ji}\vec{E}^{\,(i)j}) = 0 .$$

With this construction, we may also replace the area estimate by

$$A^{\mu\nu}_{\triangle_{ijk}}(i) = \frac{l_{ij}l_{ik}}{2}[e_\mu^{(i)j} e_\nu^{(i)k} - e_\nu^{(i)j} e_\mu^{(i)k}] , \qquad (74)$$

to order $O(a^2)$. The entire approximation procedure depends only on a consistent choice of a coordinate system at each site i. However, the accuracy of this approximation can depend on this choice. An attractive convention which is worth investigating further is to introduce Riemann normal coordinates (RNC) [25] at each site i, with the metric, $g_{\mu\nu}(x) = g_{\mu\nu}(x_i) - (1/3)\Delta x^\lambda \Delta x^\sigma R_{\mu\lambda\nu\sigma} + O(a^3)$ to help in approximating the tangent vectors.

C. Spin Structure on the Simplicial $\mathbb{S}^2$

In preparation of our numerical tests and as a simple example, we present the construction of our 2D simplicial Dirac action on $\mathbb{S}^2$. The above procedures can be tested and used on a sphere, but a far simpler approach is to realize that all geodesics are just given by great circles. Given two points on the D−dimension sphere denoted by unit vectors $\vec{r}_i$ and $\vec{r}_j$, the geodesic is parameterized simply by $\vec{x}(t) = (t\vec{r}_i + (1-t)\vec{r}_j)/|t\vec{r}_i + (1-t)\vec{r}_j|$ with tangent vectors $e^{(i)j} = \dot{x}(0)/|\dot{x}(0)|$. The entire construction is reduced to simple vector algebra in the embedded space. Other symmetric manifolds have similar embedding methods.

For the $\mathbb{S}^2$ manifold, our triangulation [3, 4] starts with an icosahedron in Fig. 7, which provides the largest subgroup of the spherical symmetry. Each one of the 20 faces is then subdivided into L^2 equilateral triangles resulting in a total of $F = 20L^2$ triangles. Next, we project each triangle onto the unit sphere and take as edge lengths the secant distances between vertices on the sphere, as illustrated in Fig. 7 for $L = 3$. This projection introduces a small deformation of the equilateral triangles, so to accurately approximate the Lagrangian, we need to compute the finite element weights. The topology of the manifold is determined by the Euler characteristic, $\chi = V - E + F = 2 - 2H = 2$ and the geometry by the table of lengths l_{ij}.
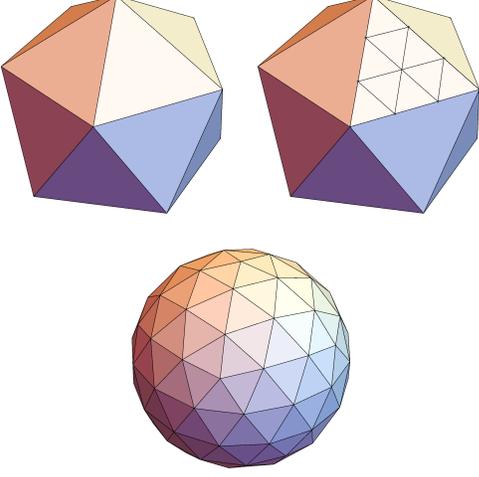
FIG. 7. The $L = 3$ refinement of the icosahedron with $V = 2 + 10L^2 = 92$ vertices or sites. The icosahedron on the top-left is refined in the top-right with $L^2 = 9$ equilateral triangles on each face, and then on the bottom the new vertices are projected onto the unit sphere. The resulting simplicial complex preserves the icosahedral symmetries.

The lattice Dirac action on $\mathbb{S}^2$ is

$$S = \frac{1}{2} \sum_{\langle i,j \rangle} \frac{V_{ij}}{l_{ij}} [\bar{\psi}_i e_a^{(i)j} \sigma^a \Omega_{ij} \psi_j - \bar{\psi}_j \Omega_{ji} e_a^{(i)j} \sigma^a \psi_i]$$

$$+ \frac{1}{2} m V_i \bar{\psi}_i \psi_i + S_{WilsonTerm} , \qquad (75)$$

where the vierbein $e_a^{(i)j} \sigma^a = e_1^{(i)j} \sigma^1 + e_2^{(i)j} \sigma^2$ are 2-vectors in the tangent plane at site i. For each link $\langle i,j \rangle$, there is a lattice spin connection, $\Omega_{ij}(\theta_{ij}) = s_{ij} e^{i\theta_{ij}\sigma_3/2}$, associated with an Abelian $O(2)$ rotation $O(\theta_{ij})$, $-\pi < \theta_{ij} < \pi$. Because we know the exact geodesics on the sphere are great circles, the geometry for the triangle $\sigma_2(ijk)$ is fixed by the set of three angles, θ_i, as shown in Fig. 8. Once $O(\theta_{ij})$ is specified, this lattice spin connection, $\Omega_{ij}(\theta_{ij})$, can then be constructed following the method in Sec. IV A.

After parameterizing the tangent plane $\vec{y} = y^a \vec{n}_a$ at each site relative to two randomly chosen orthonormal tangent vectors $\vec{n}_a$, we can determine θ_{ij} by a procedure illustrated Fig. 8. For each triangle we rotate the 1 axis at site i into a tangent vector on the arc from i to j by α_i, parallel transport this tangent vector on the geodesic to site j and rotate it back to the 1 axis at j by β_j. This gives $\theta_{ij} = \alpha_i - \beta_j$. It follows trivially that $\theta_{12} + \theta_{23} + \theta_{31} = (\theta_1 + \theta_2 + \theta_3) \mod 2\pi$, where the deficit angle is defined by

$$\delta_{123} = A_{123} = 2\pi - (\theta_1 + \theta_2 + \theta_3)$$
$$= 2\pi - (\theta_{12} + \theta_{23} + \theta_{31}) \mod 2\pi . \qquad (76)$$

Now the problem is to determine s_{ij} for all links self-consistently for the entire sphere following the procedure
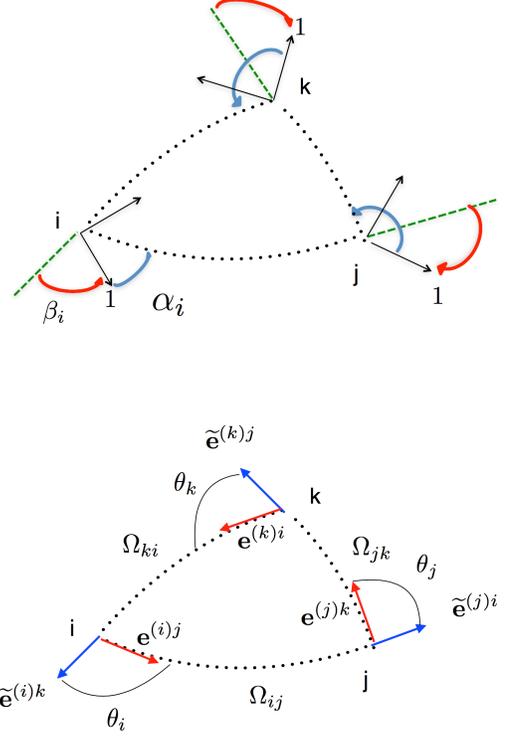
FIG. 8. On the top, vectors in the tangent planes, and on the bottom, the lattice spin connection, Ω_{12} and the outgoing and reflected vierbeins, $\mathbf{e}^{(i)j} = e_a^{(i)j}\gamma^a$ and $\widetilde{\mathbf{e}}^{(i)j} \equiv -\mathbf{e}^{(i)j}$, respectively.

described in Sec. IV A. As before, choose an arbitrary triangle and fix the signs, s_{ij}, to satisfy constraint to minimize the integrated curvature (58, then move to adjacent triangles fixing the signs s_{ij} on new edges until you encounter the last triangle. Now all the edges have fixed signs so there could be an obstruction. However, since the deficit angle is additive (or, for the sphere, the areas are additive), for any closed loop we know that this last triangle on a unit sphere, when viewed from the outside, has a deficit angle $\delta \simeq 4\pi - A_\triangle$ in steradians. But since $e^{4\pi i \sigma^3/2} = 1$, the 4π factor can be dropped and there is no obstruction.

It is a simple algebraic exercise to show this exact consistency condition on the sphere holds generally for any triangulation of a surface with the topology of a sphere. The more general argument is as follows. Assume the interior angle for the ith vertex in triangle $\triangle_{ijk}$ is given by $\widetilde{\theta}_i = \pi - \theta_i$ and that all the interior angles on the tangent plane at each vertex add up exactly to 2π. Then the deficit angle is $\delta(ijk) = \widetilde{\theta}_i + \widetilde{\theta}_j + \widetilde{\theta}_k - \pi$ and the sum

over all angles must give

$$\sum_F [\widetilde{\theta}_i + \widetilde{\theta}_j + \widetilde{\theta}_k] = 2\pi V . \qquad (77)$$

Any 2D simplicial triangulation of a closed surface implies $3F = 2E$, so we have the sum rule,

$$\sum \delta(ijk) = 2\pi V - \pi F = 2\pi(V - E + F)$$
$$= 4\pi(1 - H) , \qquad (78)$$

which for the sphere by Euler's identity gives 4π. In fact, this argument applies to any closed orientable 2D triangulation, or any surface with an even number of boundaries B, such as the cylinder. Even with an approximate determination of the angles, as for example in our relaxation algorithm in Sec. IV B, the constraint remains exact.

Finally, we should note a simple interpretation for a 2D complex Riemann manifold. In the complex plane, all Riemann manifolds can be represented by adding pairs of square root branch points. For example, a square root branch point at the origin with a cut out to infinity represents a cylinder with two open boundaries. When you add an even number of pairs, these create handles—4 twists for the torus, etc. As we discuss in Sec. VI for the simplicial Dirac equation, a pair of branch points is equivalent to allowing a pair of -1 "frustrated" triangles. In the context of Ising CFT, this corresponds to the insertion of twist operators. Just as square root branches come in pairs when you flip edges ($s_{ij} \to -s_{ij}$), on the simplicial complex it creates a pair of "frustrated" triangles. This is a nice illustration of the fact that the existence of a spin structure on a Riemann manifold is a purely topological property that is naturally encoded in the simplicial complex without the need to introduce a metric.

V. NUMERICAL TESTS FOR 2D DIRAC FERMIONS

For simplicity, we restrict our tests to the Dirac fermion (29) on $\mathbb{S}^2$, which can be easily solved analytically [28]. For future tests, higher dimensional spherical solutions are also available, for example the 4D sphere in Ref. [28]. On $\mathbb{S}^2$, the metric is

$$ds^2_{S^2} = d\theta^2 + \sin^2 \theta \, d\phi^2 . \qquad (79)$$

With $\vec{e}_\theta = (1,0)$, $\vec{e}_\phi = (0, \sin\theta)$ and $\sqrt{g} = \sin\theta$, the only non-zero components of the spin connection, (33), are $\omega_\phi^{12} = -\omega_\phi^{21} = -\cos\theta$. The action on $\mathbb{S}^2$ is

$$S_{sphere} = \int d\phi d\theta \sin\theta \bar{\psi} \, [\sigma^1 (\partial_\theta + \frac{\cot\theta}{2})$$
$$+ \sigma^2 \frac{\partial_\phi}{\sin\theta} + m]\psi . \qquad (80)$$
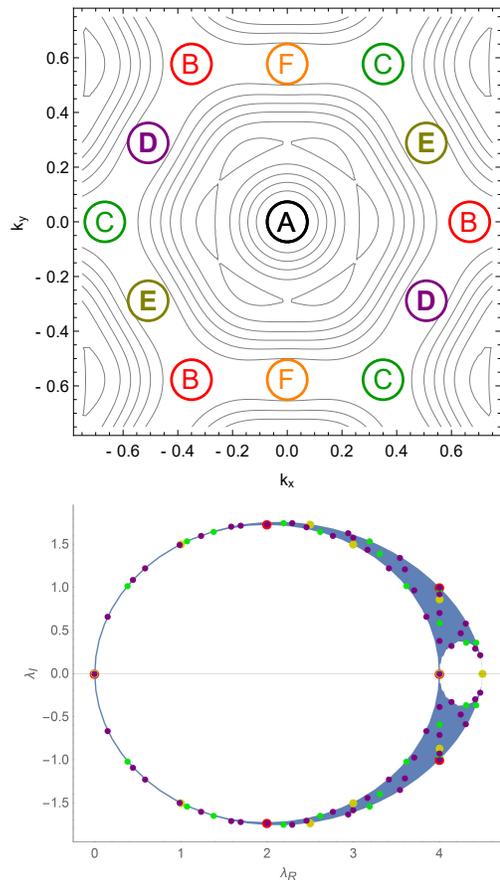
FIG. 9. On the top, the Brillouin zone for the naive Dirac operator on a regular flat triangular lattice. The zero modes are labeled A-F. On the bottom, the infinite triangular lattice spectrum with the Wilson term (solid blue) compared to small lattices with 16 (red), 36 (gold), 100 (green) and 256 (purple) sites.

The massless Dirac operator, $D = \sqrt{g}\nabla = \sin\theta[\sigma^1(\partial_\theta + \cot\theta/2) + \sigma^2(\partial_\phi/\sin\theta)]$, is anti-Hermitian and therefore has pure imaginary eigenvalues $i\lambda$. It also follows from the σ_3-Hermiticity property, $\sigma_3 D \sigma_3 = D^\dagger = -D$, that eigenvalues come in complex conjugate pairs,

$$\lambda = \pm(j + 1/2) , \qquad (81)$$

where $j = 1/2, 3/2, \cdots$ are the allowed angular momenta. Furthermore, for each j, the spectrum is $(2j + 1)$-fold degenerate [28], with the degeneracy labeled by $-j \leq m \leq j$. The explicit eigenfunctions in terms of spherical harmonics are given in Appendix B. The action is also invariant under σ_1 conjugation, $\sigma_1 D^* \sigma_1 = D$, or equivalently, together with σ_3 conjugation, $\sigma_2 D^* \sigma_2 = D^\dagger$. These discrete symmetries are *exactly* preserved on our simplicial complex.
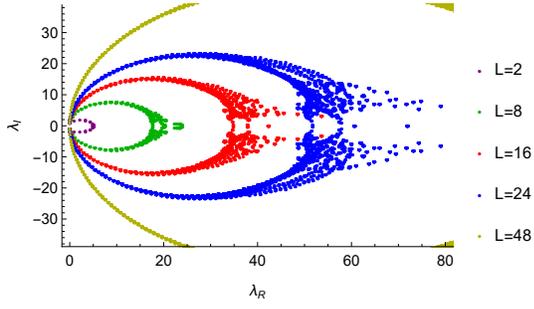
FIG. 10. The Wilson-Dirac spectra on the discrete sphere for various refinement values of the refinement L.

FIG. 11. As we increase the refinement level L, we expect the low-lying eigenvalues to converge to their continuum imaginary integer values. We see that as L increases the real part (due to the Wilson term) approaches zero and the imaginary part approaches an integer.

For comparison, on the simplicial lattice, our action is

$$S_{Dirac}^{Wilson} = \frac{1}{2} \sum_{\langle i,j \rangle} \frac{V_{ij}}{l_{ij}} \left(\bar{\psi}_i e_a^{(i)j} \sigma^a \Omega_{ij} \psi_j - \bar{\psi}_j \Omega_{ji} e_a^{(i)j} \sigma^a \psi_i \right)$$

$$+ \sum_i m V_i \bar{\psi}_i \psi_i$$

$$+ \frac{a}{2} \sum_{\langle i,j \rangle} \frac{V_{ij}}{l_{ij}^2} \left(\bar{\psi}_i - \bar{\psi}_j \Omega_{ji} \right) \left(\psi_i - \Omega_{ij} \psi_j \right) , \quad (82)$$

with the Wilson term to remove doublers. We have set the coefficient, r, of the Wilson term to the mean lattice spacing on the sphere: $r = a$. The Wilson term acts like a mass operator, so now the eigenvalues have both real and imaginary parts. Defining the lattice matrix $\mathbf{D}_{ij}$ by $S_{Wilson-Dirac} = \bar{\psi}_i \mathbf{D}_{ij} \psi_j$, σ_3 Hermiticity is still valid. Therefore, eigenvalues still come in complex conjugate pairs,

$$E = \lambda_R \pm i\lambda_I . \quad (83)$$

With rotational invariance broken, λ_I no longer takes on exactly integral values and the $(2j + 1)$-fold degeneracy is broken. In the limit of zero lattice spacing, $a \to 0$, one nevertheless anticipates the spectrum approaching $\lambda_I \to (j + 1/2)$ and $\lambda_R \to 0$, with doublers becoming increasingly massive and decoupling from the spectrum.

Before introducing the Wilson term, it is interesting to see its effect on a flat $L \times L$ regular triangular lattice with $\Omega_{ij} = 1$. In the absence of the Wilson term, as depicted by the top figure in Fig. 9, the hexagonal Brillouin zone actually has 6 copies of the 2-component spinor zero modes [29]. These zero modes are labeled as $A, B, \cdots, F$. The doublers spoil the continuum limit and even fail to restore Lorentz invariance [30]. When the Wilson term is added, the doublers are removed and the spectrum comes close to the circular complex spectrum of a lattice overlap operator [31], converging rapidly to the continuum. This is depicted in the bottom figure in Fig. 9, with the $L \to \infty$ spectrum in solid blue compared to small lattices for $L = 4, 6, 10, 16$.

On $\mathbb{S}^2$, a global view of the Wilson-Dirac spectrum is illustrated in Fig. 10. Not surprisingly, the qualitative

effects of the Wilson term on $\mathbb{S}^2$ are very similar to that for the flat lattice shown in Fig. 9. The apparent difference between the two figures as a function of the refinement L is due to our convention. On the flat plane, we treat the eigenvalues as discrete dimensionless momenta (ap^μ), which scale to a continuum dispersion relation as $a \sim 1/L \to 0$, whereas on the sphere we have fixed the radius of $\mathbb{S}^2$ to one, so the eigenvalues remain discrete approaching fixed values in the continuum limit. Fig. 10 plots the real vs imaginary parts of eigen-spectrum for increasing refinement of $L = 2, 8, 16, 24, 48$. In the limit $L \to \infty$, the imaginary parts of the low-lying eigenvalues, λ_I, approach $\pm(j + 1/2)$, while their corresponding real parts, λ_R, vanish as $O(1/L)$.

A. Spectrum of the Lattice Dirac Operator

There are two approaches to determining the spectrum of the Wilson-Dirac operator. The first is to directly evaluate the eigenvalues of the discrete Wilson-Dirac operator $\mathbf{D}_{ij}$, which is limited by the efficiency of eigenvalue routines for sparse matrices. The second approach is to assume the eigenvectors are well approximated by their continuum wave functions evaluated on the lattice sites, $\psi_i^{(n)}$, and to compute the matrix elements of the lattice Wilson-Dirac operator, $\langle \bar{\psi}^{(n)} | \mathbf{D} | \psi^{(n)} \rangle \simeq \lambda_{R,n} + i\lambda_{I,n}$. It is important to be precise in defining the spectral problem on the simplicial manifold. In the continuum the spectral problem is the stationary value of the quadratic form,

$$I = \int d^D x \sqrt{g(x)} \bar{\psi}(x) (\nabla + m - E) \psi(x) , \quad (84)$$

leading either to the conventional eigenvalue problem, $(\nabla + m)\psi(x) = E\psi(x)$, where $\nabla = \mathbf{e}^\mu \mathbf{D}_\mu$, or to the generalized eigenvalue problem $D\psi(x) = E\sqrt{g(x)}\psi(x)$ where $D = \sqrt{g}(\mathbf{e}^\mu \mathbf{D}_\mu + m)$. On the simplicial lattice, based on the discrete simplicial quadratic form,
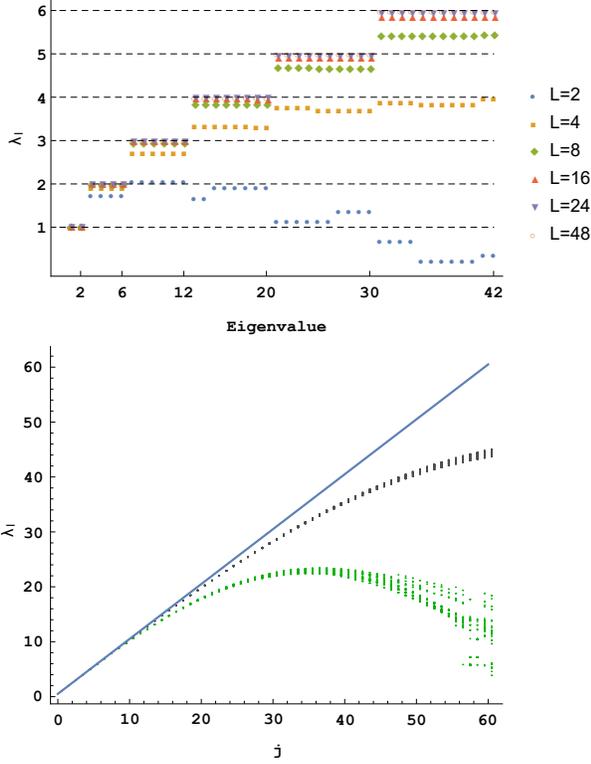
FIG. 12. On the top, we show the imaginary part of the low-lying eigenvalues, with degenerate states repeated, for various refinements. On the bottom, we show how the imaginary part of the eigenvalues for $L = 24$, in green, and $L = 48$, in grey, approach the continuum as a function of j.

FIG. 13. On the top, we show the real part of the eigenvalues for $j \leq 20$, averaged over m, at $L = 48$. On the bottom, we show a similar plot for the imaginary part of the eigenvalues. The overlaid curves reflect the asymptotic continuum behavior given in Eq. (86).

$I = \bar{\psi}_i(D_{ij} - EV_i\delta_{ij})\psi_j$, is more conveniently given as the generalized eigenvalue problem,

$$D_{ij}\psi_j^{(n)} = E_n V_i \psi_i^{(n)} \quad , \quad \overline{\sum_i} V_i \bar{\psi}_i^{(n')} \psi_i^{(n)} = \delta_{n',n} . \quad (85)$$

Here the continuum measure, $\sqrt{g(x)}$, is replaced by the Vorioni dual volume $V_i \equiv |\sigma_1^*(i)|$. Alternatively one may rescale by the square root of the measure, redefining the matrix as $\widetilde{D}_{ij} = V_i^{-1/2} D_{ij} V_j^{-1/2}$ and eigenvectors as $\widetilde{\psi}_i^{(n)} = V_i^{1/2} \psi_i^{(n)}$ to convert it to a conventional eigenvalue problem. Either way, properly treating the measure V_i is critical to a faithful correspondence with the continuum.

Lattice Eigenvalues: The low-lying eigenvalues are plotted in Fig. 11 for a range of refinements L. The black stars on the left side of the plot correspond to the continuum results for the low-lying eigenvalues of the continuum Dirac operator, which have integer spacing along the imaginary axis. The nth level has $2n$ degenerate eigenvalues corresponding to the $2j+1$ values for the magnetic quantum number, m. On the right side of the plot, we show the numerically computed spectrum for a range of refinements, $L = 2, 8, 16, 24, 48$, with $\lambda_R < 10$. The degeneracy in m is (partially) broken, but too small to be seen.

In Fig. 12, we provide a more detailed picture of the breaking of degeneracy in m. The top figure shows the imaginary part of all low-lying eigenvalues, with $1 \leq \lambda_I \leq 6$, and $\lambda_R < 10$, as L increases. As the lattice is refined, these levels quickly fall into clusters which can be associated with our continuum pattern, labeled by j-values, with an approximate degeneracy of $2j+1$. The *first three* levels are *exactly* degenerate due to the symmetry of the icosahedron under the subgroup of rotations. In the bottom figure, we see that the imaginary part of the spectrum is linear for small j and degenerate. However, for larger j, the degeneracy in m breaks down, as indicated by a spread in the eigenvalues for fixed j, and various levels overlap.

The dispersion relation including contributions from both the Dirac and the Wilson term, which should converge to

$$\lambda_I \to j + 1/2 \,, \qquad \lambda_R \to ((j+1/2)^2 - 1/2)/L, \quad (86)$$

as we approach the continuum. Here the eigenvalues are
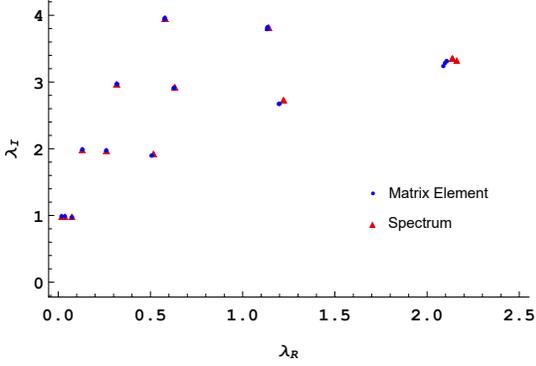
FIG. 14. A comparison of the spectrum computed via a numerical eigensolver with the spectrum computed via matrix elements for $L = 4, 8$, and 16.
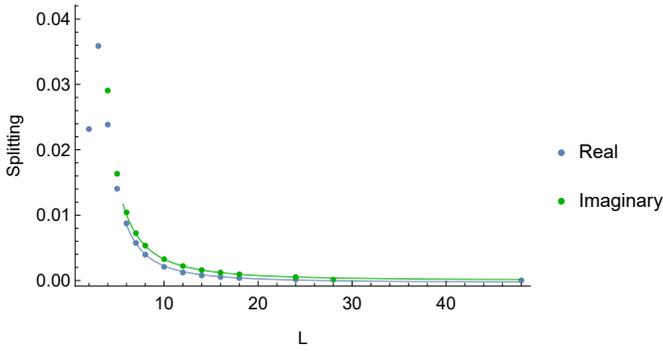
FIG. 15. The splitting of the eigenvalues for $\lambda = 4$ as a function of L. We note that with increased refinement, the eigenvalues become more degenerate.

FIG. 16. On the top, we show the approach of the imaginary part of the $\lambda = 4$ eigenvalues, averaged over m, to the continuum as a function of the refinement L. On the bottom, we show the analogous plot for the real part of the eigenvalues.

averaged over the $2j + 1$ values for the azimuthal angular momentum, m. In Fig. 13, for $L = 48$, we plot the real and imaginary parts of the eigen-spectrum as a function of j for $0 < j < 20$. For $j \leq 15/2$, we performed unweighted least-squares regression to the imaginary and real parts of the eigenvalues. For the imaginary and real parts, we find $\lambda_I(j) = 1.011(j + 0.480) - 0.00197j^2$ and $\lambda_R(j) = (0.9836j(j + 1) - 0.27 + 0.00097j^3)/L$ respectively. Both are consistent with the theoretical expectation given in Eq. (86) derived in Appendix B.

Lattice Eigenvectors: Given the continuum eigenfunctions restricted to the lattice $\psi^{(n)}$ lattice, we can in principle approximate the eigenvalue from matrix elements $\langle \psi^{(n)} | \mathbf{D} | \psi^{(n)} \rangle \simeq \lambda_{R,n} + i\lambda_{I,n}$. This also checks the accuracy of matching lattice eigenvectors to the continuum (B7). However, before proceeding, one must transform them from the continuum coordinate gauge into the gauge defined by our lattice action.

To fix the gauge, we can take advantage of the exact degeneracy in the magnetic quantum number for the first three levels. For simplicity, we choose the two lowest continuum wave functions, that is, $m = \pm 1/2$

for $j = 1/2$, discretized on to the lattice sites, $\psi_i = (\psi^{(1)}(r_i), \psi^{(2)}(r_i))^T$ compared to the corresponding lattice eigenvectors of $\Psi_i = (\Psi_i^{(1)}, \Psi_i^{(2)})^T$ for $\mathbf{D}_{ij}$. The desired gauge transformation at each site can be specified by a local spinor rotation, $e^{i\theta_i \sigma_3 / 2}$, and a global 2 by 2 unitary matrix, $\mathbb{U}$, which mixes the degenerate pair. These are determined by minimizing the functional

$$G(\theta_i, \mathbb{U}) = \sum_i \left| \psi_i - e^{i\frac{\theta_i}{2}\sigma_3} \mathbb{U} \Psi_i \right|^2 \tag{87}$$

$$= -\sum_i \overline{\psi}_i e^{i\frac{\theta_i}{2}\sigma_3} \mathbb{U} \Psi_i - \sum_i \overline{\Psi}_i^{(n)} \mathbb{U}^\dagger e^{-i\frac{\theta_i}{2}\sigma_3} \psi_i$$

with respect to $\mathbb{U}$ and $e^{i\theta_i \sigma_3 / 2}$ on each site i. This enables us to take the matrix element $\langle \overline{\psi}^{(n)} | \mathbf{D} | \psi^{(n)} \rangle$ using the discretize continuum eigenvector rotated to our lattice frame to estimate the eigenvalues. In Fig. 14 we compare the lattice operator eigenvalues to the matrix elements. The two results are in remarkable agreement, suggesting that the discrete Wilson term has eigenvectors consistent with the Dirac term. We found that the minimum of the function G given in Eq. (87) approaches zero as $1/L^2$. This suggests that the lattice eigenvectors become an increasingly good approximation of the continuum eigenvectors as L increases. This is also consistent with our previous observation that the Wilson term, while crucial to removing spurious doublers, has a negligible effect on the physical states as $L \to \infty$.

B. Rate of Convergence to the Continuum

There are two ways to test the convergence of the spectrum to the continuum limit. **i.)** The restoration of degeneracy in the magnetic quantum number, m, as L increases. **ii.)** The behavior of the spectrum, averaged over m, as L increases. The *exact* σ_1 symmetry results in a pairing of degenerate eigenvalues for each j. Since our discretization exactly preserves icosahedral symmetry, the first level which exhibits breaking of the degeneracy in m is the fourth level. For $\lambda = 4$, there are two irreducible representations of the icosahedral group, resulting in a splitting into two groups with two and six members as illustrated on the top in Fig. 12. At higher levels, the eigenvalues can split into a larger set of irreducible representations.

Restricting our attention to $\lambda = 4$, we define the splitting in the eigenvalues, independently for the real and imaginary parts, as the difference between the maximum and minimum eigenvalues. In Fig. 15, we consider this splitting as L increases. We perform an unweighted linear regression to the splitting as a function of L. For the imaginary and real parts, we find the splitting behaves as $-6 \times 10^{-5} + 0.0034/L + 0.230/L^2$ and $0.0009 - 0.035/L + 0.44/L^2$, respectively, consistent with restoration of full spherical symmetry in the continuum.

Next we consider how the eigenvalues, averaged over m, approach the continuum for $\lambda = 4$. In Fig. 16, on top, we fit the eigenvalue to $\lambda_{I,4} = 3.99932 + 0.034/L - 11.67/L^2$ consistent with the continuum value, $\lambda_{I,4} = 4$. On the bottom, we see the real part also approaches the correct continuum value, $\lambda_{R,4} = 0$. The convergence of this term is governed by the Wilson term, which scales with an extra factor of lattice spacing compared to the naive Dirac term. We therefore expect it to converge more slowly, as $O(1/L)$. Our fit gives $\lambda_{R,4} = 0.0025 + 9.19/L$, again consistent with our expectations.

VI. THE ISING CONFORMAL FIELD THEORY ON $\mathbb{S}^2$

The exact solution to the 2D Ising model provides a rigorous test of our simplicial construction of the free fermions on $\mathbb{S}^2$. To begin let us review this continuum $c = 1/2$ minimal model. There are only three Virasoro primaries $\mathbf{1}, \sigma, \epsilon$, with an OPE expansion,

$$\sigma \times \sigma = \mathbf{1} + \epsilon, \quad \epsilon \times \sigma = \epsilon, \quad \epsilon \times \epsilon = \mathbf{1} . \quad (88)$$

It is equivalent to a free Majorana holomorphic, $\psi(z)$, and anti-holomorphic, $\bar{\psi}(\bar{z})$, field on all 2D Riemann surfaces [32]. In the complex plane, the Riemann surface can be represented by inserting pairs of square root branch points whose locations corresponds to the $\sigma(z)$ operators. When projected onto our simplicial lattice on $\mathbb{S}^2$, these represent pairs of branch points given by simplicies with curvature defects of -1. Clearly, these defects must be

inserted in pairs by flipping bonds on an invisible string between these flipped plaquettes. Here we compute the 2-point and 4-point functions,

$$\langle \epsilon(x_1)\epsilon(x_2) \rangle, \quad \text{and} \quad \langle \sigma(x_4)\epsilon(x_3)\epsilon(x_2)\sigma(x_1) \rangle, \quad (89)$$

where $\epsilon(x) = i\bar{\psi}(x)\psi(x)$ and $\sigma(x)$ is the twist operator that introduces the square root branch points. Of course, correlators with only fermion operators, such as $\langle \epsilon(x_1)\epsilon(x_2)\epsilon(x_3)\epsilon(x_4) \rangle$, are trivially given by the Wick contractions as products of 2-point functions $\langle \epsilon(x_1)\epsilon(x_2) \rangle$. The $\langle \sigma(x_4)\sigma(x_3)\sigma(x_2)\sigma(x_1) \rangle$ correlation function is the partition function on the torus. This is computed in Ref. [5] as a test of QFE methods for the ϕ^4 CFT theory on $\mathbb{S}^2$.

A. Dirac vs Majorana Propagators

In the continuum, the 2D Dirac fermion,

$$S = \int d^2x \bar{\Psi}[\sigma^\mu \partial_\mu + m]\Psi$$
$$= 2 \int dz d\bar{z} \bar{\Psi}[\sigma_- \partial_{\bar{z}} + \sigma_+ \partial_z + m]\Psi , \quad (90)$$

at zero mass can be decomposed into two single component Majorana fermions,

$$S = 2 \int dz d\bar{z}[\psi \partial_{\bar{z}} \psi + \bar{\psi} \partial_z \bar{\psi}]$$
$$= 2 \int dz d\bar{z}[\psi \bar{\partial} \psi + \bar{\psi} \partial \bar{\psi}] , \quad (91)$$

where $\Psi = (\Psi_1, \Psi_2)^T \equiv (\psi, \bar{\psi})$ and $\bar{\Psi} = \Psi^T \sigma^1 = (\Psi_2, \Psi_1)^T \equiv (\bar{\psi}, \psi)$ are split into a holomorphic and anti-holomorphic parts, $\psi(z)$ and $\bar{\psi}(\bar{z})$, respectively. The holomorphic propagator is

$$\langle \psi(z_1)\psi(z_2) \rangle = \langle z_1, \bar{z}_1 | \bar{\partial}^{-1} | z_2, \bar{z}_2 \rangle \quad (92)$$
$$= \partial \langle z_1, \bar{z}_1 | (\bar{\partial}\partial)^{-1} | z_2, \bar{z}_2 \rangle = \frac{1}{2\pi} \frac{1}{z_1 - z_2} ,$$

and the anti-holomorphic propagator is $\langle \bar{\psi}(\bar{z}_1)\bar{\psi}(\bar{z}_2) \rangle = \langle \psi(z_1)\psi(z_2) \rangle^*$. Note that these solutions are regular at 0 and ∞, and periodic in $\theta \to \theta + 2\pi$ for $z = |z|e^{i\theta}$. By inserting twist operators at 0 and ∞, the propagators,

$$\langle \sigma(\infty)\psi(z_1)\psi(z_2)\sigma(0) \rangle = \frac{\sqrt{\frac{z_1}{z_2}} + \sqrt{\frac{z_2}{z_1}}}{4\pi} \frac{1}{z_1 - z_2} , \quad (93)$$

and $\langle \sigma(\infty)\bar{\psi}(\bar{z}_1)\bar{\psi}(\bar{z}_2)\sigma(0) \rangle = \langle \sigma(\infty)\psi(z_1)\psi(z_2)\sigma(0) \rangle^*$ are now anti-periodic in θ. To make contact with our simplicial Dirac fermion requires two steps: first projecting the flat space correlators to the Riemann $\mathbb{S}^2$ sphere and second identifying a single Majorana component within our 2 component simplicial Dirac fermion.

B. Stereographic Projection for Conformal Fields

Under a Weyl rescaling of the flat metric,

$$g_{\mu\nu}(x) = \frac{\partial \xi^\alpha}{\partial x^\mu} \frac{\partial \xi^\alpha}{\partial x^\nu} = \Omega^2(x)\delta_{\mu\nu} \ , \tag{94}$$

the conformal correlation functions for primaries $\mathcal{O}_i$ of dimension Δ_i obey the general identity [33],

$$\langle \mathcal{O}_1(x_1)\mathcal{O}_2(x_2)\cdots\rangle_{g_{\mu\nu}} \tag{95}$$
$$= [\frac{1}{\Omega(x_1)^{\Delta_1}} \frac{1}{\Omega(x_2)^{\Delta_2}} \cdots]\langle \mathcal{O}_1(\xi_1)\mathcal{O}_2(\xi_2)\cdots\rangle_{flat} \ .$$

In particular the map, $\mathbb{R}^2 \to \mathbb{S}^2$, to the projective sphere,

$$ds_{\mathbb{S}^2}^2 = \frac{2}{(1+z\bar{z})^2} dz d\bar{z} = \cos^2(\theta/2)ds_{\mathbb{R}^2}^2 \ . \tag{96}$$

introduces the Weyl factor, $\Omega^2(\theta) = \cos^2(\theta/2)$, and leads to the identity for the 2 point function

$$\langle \mathcal{O}_1(x_1)\mathcal{O}_2(x_2)\rangle_{\mathbb{S}^2} = \frac{1}{[\Omega(x_1)|z_1 - z_2|^2\Omega(x_2)]^\Delta}$$
$$= \frac{1}{(2 - 2\cos\theta_{12})^\Delta} \ , \tag{97}$$

where $\Omega(\theta_1)|z_1 - z_2|^2\Omega(\theta_2) = |\vec{r}_1 - \vec{r}_2|^2 = 2(1 - \cos\theta_{12})$ with radial vectors, $r = (r_x + ir_y, r_z) = (\sin\theta e^{i\phi}, \cos\theta)$ restricted to the unit sphere embedded in $\mathbb{R}^3$. Just as Poincare invariance on the plane implies that correlators are a function of the length (or Euclidean distance on the plane, $|z_1 - z_2|$), rotational invariance on the sphere fixes the correlator to be a function of the geodesic distance, θ_{12}. In addition scale invariance fixes the full functional form.

It is often useful to make use of conformal cross ratios u and v, which are also invariant under Weyl transformations,

$$u = \frac{x_{12}^2 x_{34}^2}{x_{13}^2 x_{24}^2} = \frac{r_{12}^2 r_{34}^2}{r_{13}^2 r_{24}^2} \quad , \quad v = \frac{x_{14}^2 x_{32}^2}{x_{13}^2 x_{24}^2} = \frac{r_{14}^2 r_{32}^2}{r_{13}^2 r_{24}^2} \ , \tag{98}$$

where $r_{ij}^2 = (\vec{r}_i - \vec{r}_j)^2 = 2(1 - \cos\theta_{ij})$. In moving from $\mathbb{R}^2$ to $\mathbb{S}^2$, all conformal factors cancel. In 2D one also can combine the two cross ratios into a single complex number,

$$\zeta = \frac{(z_1 - z_2)(z_3 - z_4)}{(z_1 - z_3)(z_2 - z_4)} \ , \tag{99}$$

where $z_i = \cot(\theta_i/2)e^{i\phi_i}$ and $u = |\zeta|^2, v = |1 - \zeta|^2$.

For future reference, we point out that this construction can be generalized to $\mathbb{S}^D$ by the replacement $\hat{r} = (r_z, \vec{r}_\perp) = (\cos\theta, \sin\theta\,\hat{r}_\perp)$, or if you prefer use rotational symmetry to bring r_z and $|\vec{r}_\perp|$ to the $x - y$ plane. One may see this in two steps. First, one maps $\mathbb{R}^D \to \mathbb{R} \times \mathbb{S}^{D-1}$ via radial quantization with coordinates $(\log r, \vec{r}_\perp)$, then one maps to the projective sphere $\mathbb{R} \times \mathbb{S}^{D-1} \to \mathbb{S}^D$ with coordinates $(\cos\theta, \sin\theta\hat{r}_\perp)$.

C. Numerical Tests for 2-and 4-Point Correlators

To numerically compute conformal correlators, we need to identify the Majorana components in our simplicial Wilson Dirac fermions. This is accomplished by including a Majorana mass, and comparing the continuum with the lattice form of the Dirac operators,

$$M_{z_1,z_2} = \begin{bmatrix} m & \partial \\ \bar{\partial} & m \end{bmatrix}_{z_1,z_2} \to \begin{bmatrix} W & \nabla \\ -\nabla^\dagger & W \end{bmatrix}_{z_1,z_2} \ . \tag{100}$$

On the right, ∇ is the naive central difference operator for a massless lattice fermion and W is the Wilson term including the mass. This identification recognizes that the Wilson term W plays the role of the mass term in the continuum limit, in addition to removing the unphysical doublers. We compute the inverse for both representations using the Schur decomposition. In the continuum, on $\mathbb{R}^2$, we have the expression,

$$G(z_1, z_2; m) \tag{101}$$
$$= \begin{bmatrix} m^{-1}(1 + \partial(m^2 - \bar{\partial}\partial)^{-1}\bar{\partial}) & -\partial(m^2 - \bar{\partial}\partial)^{-1} \\ -(m^2 - \bar{\partial}\partial)^{-1}\bar{\partial} & m(m^2 - \bar{\partial}\partial)^{-1} \end{bmatrix} \ ,$$

for $G(z_1, z_2; m) = M_{z_1,z_2}^{-1}$, which can be compared with the Wilson Dirac lattice propagator,

$$G(z_1, z_2) \tag{102}$$
$$= \begin{bmatrix} W^{-1}(1 + \nabla\boldsymbol{\Delta}_s^{-1}\nabla^\dagger W^{-1}) & -W^{-1}\nabla\boldsymbol{\Delta}_s^{-1} \\ \boldsymbol{\Delta}_s^{-1}\nabla^\dagger W^{-1} & \boldsymbol{\Delta}_s^{-1} \end{bmatrix}_{zw} \ ,$$

where $\boldsymbol{\Delta}_s = W + \nabla^\dagger W^{-1}\nabla$ is the Schur complement. Taking the zero mass limit of Eq. (102), we can identify the Majorana propagator as the off-diagonal terms in Eq. (103), so it follows that on the lattice, we should also identify these off-diagonal term for the lattice conformal propagators. Consequently, in the zero mass limit, the correspondence,

$$G_{12}(z_1, z_2)G_{21}(z_1, z_2) = |G_{12}(z_1, z_2)|^2$$
$$\to \langle \psi(z_1)\bar{\psi}(\bar{z}_1)\bar{\psi}(\bar{z}_2)\psi(z_2)\rangle \ , \tag{103}$$

is established.

Lattice $\epsilon\epsilon$ Correlator: We will now show numerically that not only is Eq. (103) correct, but the simplicial correlator converges rapidly to the continuum on $\mathbb{S}^2$,

$$\langle \epsilon(\vec{r}_1)\epsilon(\vec{r}_2)\rangle = \frac{1}{4\pi^2} \frac{1}{2(1 - \cos\theta_{12})} \ . \tag{104}$$

A comparison of the numerical result versus the analytic result is given in Fig. 17. At very small distances, cutoff effects give a visible disagreement with the continuum result, but otherwise the fit is remarkably good even at relatively small $L = 16$. It is important to note that this is a zero parameter fit, including the normalization. Fitting the data to the expected functional form, we find $(a/8\pi^2) \times (1 - \cos\theta)^{-\gamma} \simeq (1.0035/8\pi^2) \times (1 - \cos\theta)^{-0.996}$. At $L = 16$ the finite lattice errors are less than 1 per cent.
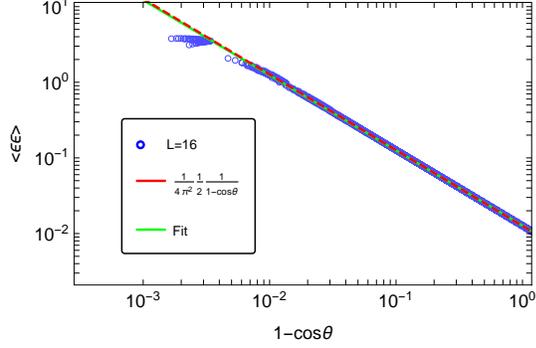
FIG. 17. Log-Log plot of the two point correlator for $L = 16$.
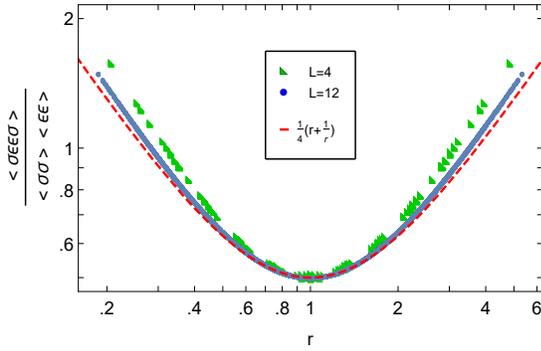
FIG. 18. Functional dependence in r of the four point correlator for $L = 4, 8, 12$, isolated by subtracting the θ term. The dotted red line is the expected continuum behavior.

Lattice $\sigma\epsilon\epsilon\sigma$ Correlator: To examine the four-point correlator, we need to introduce twist operators on the lattice. It is convenient to introduce the branch points at the north and south poles of our decorated icosahedron and to maintain a discrete 5-fold axial symmetry in θ. To accomplish this, first, the pole points are removed. This
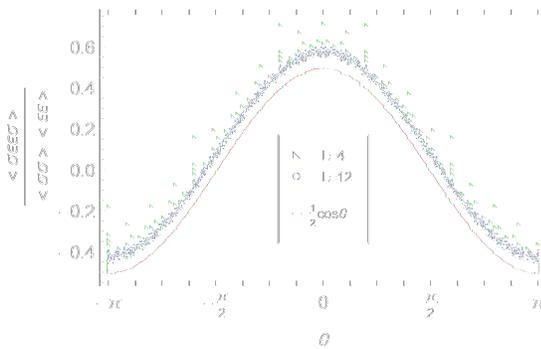
FIG. 19. Functional dependence in θ of the four point correlator for $L = 4, 8, 12$ isolated by subtracting the r terms. The dotted red line is the expected continuum behavior.

takes our lattice from the topology of a sphere to the cylinder. Next, the spin connection on one link around the poles is flipped in sign. This introduces a topological defect at the north and south poles which corresponds to the insertion of our lattice twist operators. Finally, a path is constructed between the flipped links at the north and south poles, flipping the sign of the spin connection along the path, so that the only defects are at the north and south poles.

For a numerical comparison we normalize the lattice four point function by the simplicial lattice two point function and compare with the analytical form on the sphere,

$$\frac{\langle\,\sigma(\infty)\epsilon(z_2)\epsilon(z_3)\sigma(0)\,\rangle}{\langle\,\epsilon(z_2)\epsilon(z_3)\,\rangle} = \frac{1}{4}(r + 1/r + 2\cos\theta_{23})\,,\quad(105)$$

as a function of the conformally invariant co-ordinate: $z_2/z_3 \equiv re^{i\theta}$. Unlike the 2-point function, this depends on both the angular separation θ_{23} and the magnitude $|z_2/z_3|$. When either one of the ϵ operators is near the poles, the ratio function in Eq. (105) diverges and the lattice results have strong cut-off effects, which we suppress by restricting the ϵ fields to the range between polar angles $[\pi/4, 3\pi/4]$. The results can be seen in Figs. 18 and 19. First, in Fig. 18, we see the r dependence of the ratio function by subtracting off the $\cos(\theta)/2$ data, and next in Fig. 19 we see the θ dependence by subtracting off the $(r + 1/r)/4$ data. In both cases, the numerical results converge to the continuum result shown in red. The total data set can be fit to the functional form $a(r + 1/r)/4 + b\cos(\theta)/2$ with $1/L$ corrections giving $a = 1.0008 + 0.264/L$ and $b = 1.00033 - 0.00566/L$. In view of the neglecting $O(1/L^2)$ terms in the fit, this is consistent with the exact continuum limit ($a = b = 1$).

VII. DISCUSSION AND FUTURE DIRECTIONS

We have presented a solution to lattice Dirac fermions on a simplicial complex approximating a general smooth Riemann manifold. To achieve this we borrowed methods from Finite Elements (FEM), Regge Calculus (RC) and the language of the Discrete Exterior Calculus (DEC). However, our solution required substantial new features to accommodate the curved manifold going beyond the linear piecewise implementations prevalent in the literature. To remove the doublers, we have used the construction of Wilson fermions. As in flat space, the operator for this simplicial Wilson fermion can be used as a kernel for Shamir [34] and Möbius [35] Domain Wall fermions by introducing a flat extra dimension of length L_s. Just as in flat space, this should converge as $L_s \to \infty$ to an exact simplicial lattice chiral overlap fermion representation [31].

This appears to us to be the first general solution for simplicial lattice Dirac fermions on any smooth Euclidean Riemann manifold that is capable of convergence to the exact continuum limit. To support this conjecture,

tests were made for the simplicial lattice on a 2D Riemann sphere compared with the exact continuum solutions. While this is obviously far from a proof, additional tests on higher dimension manifolds will be performed. The proof of convergence theorems have not yet been attempted. Convergence proofs for classical FEM and Regge Calculus are far from trivial or complete [8], let alone their extension to the simplicial fermions presented here. However, we feel that the geometrical underpinning of our approach makes our convergence conjecture plausible.

To address the central problem of Quantum Finite Elements (QFE), interacting quantum field theory on curved manifolds, we need to introduce interactions with scalar and gauge fields. Yukawa terms interacting with scalars are not difficult to formulate using linear FEM truncated to local terms to represent a minimal set of relevant operators. The inclusion of gauge fields interacting with our simplicial lattice fermions is also straightforward for vector like theories by replacing the spin connection Ω_{ij} on each link by the product $\Omega_{ij}U_{ij}$ in the action for the Dirac field,

$$S_{Wilson} = \frac{a}{2} \sum_{\langle i,j \rangle} \frac{V_{ij}}{l_{ij}^2} (\bar{\psi}_i \hat{e}_a^{j(i)} \gamma^a \Omega_{ij} U_{ij} \psi_j \qquad (106)$$
$$-\bar{\psi}_j \Omega_{ji} U_{ji} \hat{e}_a^{i(j)} \gamma^a \psi_i) + \cdots ,$$

where U_{ij} is the Wilson compact gauge link matrix,

$$U_{ij} = e^{\,il_{ij}^\mu A_{ij}^\mu} , \qquad (107)$$

and $A_{ij} = \lambda^a A_{ij}^a$ is the non-Abelian gauge potential. The kinetic term in the action has been considered in Ref. [10] in flat space, but can be easily introduced on our simplicial manifold as well. The continuum action

$$S = \frac{1}{2} \int d^D x \sqrt{g} \, g^{\mu\nu'} g^{\mu'\nu} F_{\mu\nu}^a(x) F_{\mu'\nu'}^a(x) , \qquad (108)$$

is replaced by a finite element action as sum over all triangles,

$$S_\sigma = \frac{1}{2g^2 N_c} \sum_{\triangle_{ijk}} \frac{V_{ijk}}{A_{ijk}^2} Tr[2 - U_{\triangle_{ijk}} - U_{\triangle_{ijk}}^\dagger] \qquad (109)$$

where where $A_{ijk} = |\sigma_2(ijk)|$ is the area of the triangle for the plaquette, $V_{ijk} = |\sigma_2(ijk) \wedge \sigma_2^*(ijk)|$ is the dual volume element, and the gauge matrix on each plaquette is the product $U_{\triangle_{ijk}} = U_{ij}U_{jk}U_{ki}$. The reader is referred to Ref. [10] for the demonstration that this has the correct continuum limit.

The quantum field path integral on a simplicial lattice requires confronting UV divergences with additional counter terms as we will report in Ref. [13]. Progress has been made for the Wilson-Fisher conformal fixed point in ϕ^4 theory by explicitly computing a finite number of UV divergent diagrams on the simplicial lattice. The extension of this approach to other super-renormalizable theories appears promising, opening up a new approach

to lattice field theory with a view towards implementing 3D lattice radial quantization. There are also many other interesting CFTs to explore by developing code and algorithms similar to those in common use. Our plan is to identify the geometrical properties of counter terms and, if possible, develop the full QFE path integral in 4D, but we recognize that this is a difficult problem. We are optimistic that we will be able to achieve this within our current QFE methodology via a single sequence of refined simplicial lattices approaching the continuum Riemann manifold for UV complete field theories. The guiding principle is to formulate non-perturbative renormalization schemes similar to methods develop for lattice field theory in flat space with the geometrical classification of the counter terms required in perturbative renormalization on Riemann manifold [36, 37]. Other approaches such as a quenched ensemble of simplicial lattices constrained to the target manifold as advocated in the random lattice program [38] for flat space may warrant further investigation in spite of their increased computational complexity.

Appendix A: Dirac Finite Element

The construction of our new piecewise flat Dirac finite element described in Sec. III A proceeds in the following steps. We seek a new finite expansion on each triangle $\triangle_{123}$

$$\psi(x) = E^1(x)\psi_1 + E^2(x)\psi_2 + E^3(x)\psi_3 ,$$
$$\bar{\psi}(x) = E^1(x)\bar{\psi}_1 + E^2(x)\bar{\psi}_2 + E^3(x)\bar{\psi}_3 . \qquad (A1)$$

in terms of the new Elements, $E^i(x)$, which satisfy 3 conditions: **(i)** The faithful interpolation of the Dirac field requires $E^i(x = r_j) = \delta_j^i$, at each vertex $x = r_j$, **(ii)** the preservation of constant fields $E^1(x) + E^2(x) + E^3(x) = 1$, and **(iii)** the lattice Dirac equation propagates on each link $\langle i,j \rangle$ with the spin matrix $\vec{l}_{ij} \cdot \vec{\sigma}$. Surprisingly, all three constraints have a simple solution in terms of three
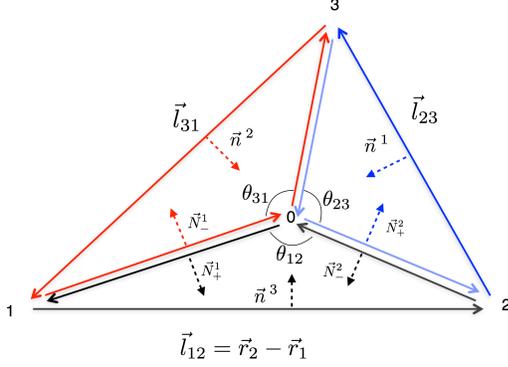
FIG. 20. Each triangle on the simplicial lattice given by the $\triangle_{123}$ with vertices $\vec{r}_1, \vec{r}_2, \vec{r}_3$ is divided into 3 isosceles sub-triangles meeting at the circumcenter at 0.

sub-triangles with linear elements meeting at the circumcenter with a ghost field

$$
\begin{aligned}
\psi_0 &= c_1\psi_1 + c_2\psi_2 + c_3\psi_3 \quad, \\
\bar{\psi}_0 &= c_1\bar{\psi}_1 + c_2\bar{\psi}_2 + c_3\bar{\psi}_3 \; ,
\end{aligned} \tag{A2}
$$

given as a linear function of the values at the vertices. The calculation requires computing the action and applying these constraints to determine the values of the coefficients c_i.

The basic algebra relies on the geometry illustrated in Fig. 20 by vectors/dual-vectors, $(\vec{l}_{ij}, \vec{n}^{\,k})$. The simplex for $\triangle_{123}$ has normal vectors $(\vec{n}^{\,1}, \vec{n}^{\,2}, \vec{n}^{\,3})$. In addition, each of the sub-triangle have the normals $(\vec{N}_+^i, \vec{N}_0^i, \vec{N}_-^{i+1})$, where the normal on the exterior links, $\vec{N}_0^i$, are just rescaled from $\vec{n}^{\,i}$ by $\vec{N}_0^i = (A_{123}/A_{0i,i+1})\,\vec{n}^{\,i}$. As a consequence we have the sum rules

$$
\begin{aligned}
\vec{N}_+^i + \vec{N}_0^i + \vec{N}_-^{i+1} &= 0 \; , \\
A_{023}\vec{N}_0^1 + A_{031}\vec{N}_0^2 + A_{012}\vec{N}_0^3 &= 0 \; .
\end{aligned} \tag{A3}
$$

In addition, normals to a shared link for two adjacent sub-triangles are related by $A_{0,i-1,i}\vec{N}_-^i + A_{0,i,i+1}\vec{N}_+^i = 0$. All of these relations hold for an arbitrary location for the center vertex 0.

Restricting vertex 0 to the circumcenter leads to three isosceles sub-triangles and there are now additional geometrical constraints. Within each sub-triangle, the sum and difference of $\vec{N}_+^i$ and $\vec{N}_-^{i+1}$ are perpendicular and parallel to the opposite link vector, $\vec{l}_{i,i+1}$, respectively, i.e.,

$$
\vec{l}_{i,i+1}\cdot(\vec{N}_+^i+\vec{N}_-^i) = 0 \quad , \quad \vec{N}_+^i - \vec{N}_-^{i+1} = \frac{2\vec{l}_{i,i+1}}{l_{i,i+1}^2} \; . \tag{A4}
$$

Applying the linear FEM interpolation formula, Eq. (39),

to each sub-triangle $\Delta_{0,i,i+1}$ we have,

$$
\begin{aligned}
S_{0i,i+1} \;=\; & \frac{A_{0,i,i+1}}{6}[\bar{\psi}_i(\vec{N}_i^+ - \vec{N}_{i+1}^-)\cdot\vec{\sigma}\psi_{i+1} \\
& + \bar{\psi}_{i+1}(\vec{N}_{i+2}^0 - \vec{N}_i^+)\cdot\vec{\sigma}\psi_0 \\
& + \bar{\psi}_0(\vec{N}_{i+1}^- - \vec{N}_{i+2}^0)\cdot\vec{\sigma}\psi_i\,] \\
& -\; c.c.
\end{aligned} \tag{A5}
$$

and the sum $S_{123} = S_{0,12} + S_{0,23} + S_{0,31}$, with the help of the identity, $(A_{0,i,i+1}\vec{N}_i^+ + A_{0,i+1,i+2}\vec{N}_{i+2}^-) = A_{0,i,i+2}\vec{N}_{i+1}^0$, gives

$$
\begin{aligned}
S_{123} = \; & \tfrac{1}{3}\sum_i A_{0,i,i+1}[\bar{\psi}_i(\vec{N}_i^+ - \vec{N}_-^{i+1})\cdot\vec{\sigma}\psi_{i+1} \\
& \qquad - \bar{\psi}_{i+1}(\vec{N}_+^i - \vec{N}_-^{i+1})\cdot\vec{\sigma}\psi_i] \\
& + \tfrac{1}{3}\sum_i A_{0,i-1,i+1}[\bar{\psi}_i\vec{\sigma}\cdot\vec{N}_0^i\psi_0 - \bar{\psi}_0\vec{\sigma}\cdot\vec{N}_0^i\psi_i] \; .
\end{aligned} \tag{A6}
$$

Introducing the expansion for the ghost field ψ_0 and $\bar{\psi}_0$, the link $\bar{\psi}_1\vec{\sigma}\psi_2$ receives contributions from both the $\bar{\psi}_1\vec{\sigma}\psi_0$ and $\bar{\psi}_0\vec{\sigma}\psi_2$ terms. We now require that each edge is properly aligned,

$$
\frac{A_{012}}{3l_{12}^2}\vec{l}_{12} - \frac{A_{031}}{3}\vec{N}_0^2 c_1 + \frac{A_{023}}{3}\vec{N}_0^1 c_2 \sim \vec{l}_{12} \tag{A7}
$$

plus permutations for the $\bar{\psi}_2\vec{\sigma}\psi_3$ and $\bar{\psi}_3\vec{\sigma}\psi_1$ links. The first term in each equation is already in the form we are seeking. Now we have what appears to be an over constrained system for three coefficients c_i satisfying the normalization constraint $c_1 + c_2 + c_3 = 1$.

An efficient approach to solving for these coefficients is to project these equations in the perpendicular direction by taking the scalar product with $\vec{N}_0^3, \vec{N}_0^1, \vec{N}_0^2$, respectively. After some algebra, using the identity $\vec{l}_{ik}\cdot\vec{l}_{kj} = 4A_{123}^2\vec{n}^{\,i}\cdot\vec{n}^{\,j}$, this reduces to a homogeneous matrix equation,

$$
\begin{bmatrix}
\vec{l}_{31}\cdot\vec{l}_{12} & -\vec{l}_{23}\cdot\vec{l}_{12} & 0 \\
0 & \vec{l}_{12}\cdot\vec{l}_{23} & -\vec{l}_{31}\cdot\vec{l}_{23} \\
-\vec{l}_{12}\cdot\vec{l}_{31} & 0 & \vec{l}_{23}\cdot\vec{l}_{31}
\end{bmatrix}
\begin{bmatrix} c_1 \\ c_2 \\ c_3 \end{bmatrix} = 0 \; . \tag{A8}
$$

As the determinant is zero, a non-trivial null vector exists, given by

$$
c_k = c_0 \frac{A_{123}}{\vec{l}_{ik}\cdot\vec{l}_{kj}} \tag{A9}
$$

for $ikj = (123)$ and cyclic, where we have expressed the solution up to a undetermined dimensionless constant c_0, which can be chosen to satisfy the normalization $c_1 + c_2 + c_3 = 1$. After considerable algebraic manipulation the final solution becomes,

$$
c_k = \frac{4A_{0ik}}{l_{ik}^2}\frac{4A_{0jk}}{l_{jk}^2} = \cot(\theta_{ik}/2)\cot(\theta_{jk}/2) \; , \tag{A10}
$$

where the vertex angle for each isosceles triangle is given by $\cot(\theta_{ij}/2) = 2h_{ij}/l_{ij} = 4A_{0ij}/l_{ij}^2$.

The consistency between Eq. (A9) and Eq. (A10) prior to this normalization requires only that the ratios c_i/c_j are unchanged which may be verified using the following set of identities. Let R be the circum-radius such that one has $l_{ij} = 2R\sin(\theta_{ij}/2)$. The total area can be expressed symmetrically as $A_{123} = l_{12}l_{23}l_{31}/4R = 2R^2\sin(\theta_{12}/2)\sin(\theta_{23}/2)\sin(\theta_{31}/2)$. The equation for the scalar product leads to:

$$\vec{l}_{ik} \cdot \vec{l}_{kj} = 4R^2 \cos(\theta_{ik}/2 + \theta_{kj}/2)\sin(\theta_{ik}/2)\sin(\theta_{kj}/2))$$
$$= 2A_{123}\cot(\theta_{ij}/2). \tag{A11}$$

The normalization condition, $c_1 + c_2 + c_3 = 1$, follows from the elegant identity,

$$\tan(\theta_{12}/2) + \tan(\theta_{23}/2) + \tan(\theta_{31}/2) \tag{A12}$$
$$= \tan(\theta_{12}/2)\tan(\theta_{23}/2)\tan(\theta_{31}/2) ,$$

for $\theta_{12} + \theta_{23} + \theta_{31} = 2\pi$. Geometrically, this identity reflects the fact that the area of the triangle equals the sum of areas of three sub-triangles, $A_{123} = A_{012} + A_{023} + A_{031}$. Remarkably, with c_i appropriately chosen, the additional two terms in Eq. (A7) are not only aligned with the first one but the sum of all three provides precisely the FEM weight for our conjectured Dirac ansatz above. It is appealing that the use of the dual vertex is necessary to the construction analogous to our Discrete Exterior Calculus formulation of the scalar. Generalizations of this construction for $D > 2$ using the dual lattice are being sought.

Let us end with two additional comments. First, if we choose $c_i = \xi_i^* = A_{0jk}/A_{123}$, we get back to the naive linear FEM result for the entire triangle Δ_{123}, which, as stated earlier, does not lead to Eq. (35). Second, if one chooses an arbitrary point 0 inside the triangle, instead of the circumcenter, it is still possible to adjust the coefficient c_i so that propagator on the links is aligned with $\vec{l}_{ij}$. However, the magnitude does not agree with our ansatz in (35), and it does not admit a simple geometrical interpretation.

Appendix B: Spectrum of the Dirac Fermion on $\mathbb{S}^2$

Here we rederive the Dirac operator on $\mathbb{S}^2$ by starting from the Dirac fermion in 4D projected to the 2 sphere. In 4D, consider the change of variables from Cartesian to spherical coordinates, $x^\mu = (t, \vec{r})$, where $\vec{r} = (r\sin\theta\cos\phi, r\sin\theta\sin\phi, r\cos\theta)$. The fermion action, $\bar{\psi}\gamma^\mu\partial_\mu\psi$, can be re-expressed as

$$\gamma^\mu\partial_\mu = \gamma_0\partial_t + \frac{1}{r}(\gamma^r\partial_{\log(r)} + \gamma^\theta\partial_\theta + \frac{1}{\sin\theta}\gamma^\phi\partial_\phi) , \tag{B1}$$

where $\gamma^r = \hat{e}_r \cdot \vec{\gamma} = \sin\theta(\cos\phi\gamma^1 + \sin\phi\gamma^2) + \cos\theta\gamma^3$, $\gamma^\theta = \hat{e}_\theta \cdot \vec{\gamma} = \cos\theta(\cos\phi\gamma^1 + \sin\phi\gamma^2) - \sin\theta\gamma^3$ and $\gamma^\phi = \hat{e}_\phi \cdot \vec{\gamma} = -\sin\phi\gamma^1 + \cos\phi\gamma^2$. The freedom to rotate tangent vectors allows one to rotate $\hat{e}_r$ to $\hat{e}^3$. This can be done by first rotating $\hat{e}_\phi$ to $\hat{e}^2$ and then rotating $\hat{e}_\theta$ to $\hat{e}^1$.

Equivalently, one rotates the fermion spinors, $\psi \to \Lambda\psi$ and $\bar{\psi} \to \bar{\psi}\Lambda^\dagger$ which then rotates $\gamma^\mu \to \Lambda^\dagger\gamma^\mu\Lambda = O^\mu_\nu\gamma^\nu$, where $\Lambda = \Lambda_{12}(\phi)\Lambda_{13}(\theta) = e^{\frac{i}{2}\phi\sigma^{12}} e^{\frac{i}{2}\theta\sigma^{13}}$. The gauge transformation picks up an additional term, $\bar{\psi}\gamma^\mu\partial_\mu\psi \to \bar{\psi}O^\mu_\nu\gamma^\nu\partial_\mu\psi + \bar{\psi}(\Lambda^\dagger\gamma^\mu\Lambda)(\Lambda^\dagger\partial_\mu\Lambda)\psi$, or spin connection so the Dirac operator in this frame is

$$e^\mu_c\gamma^c(\partial_\mu + \frac{1}{4}\omega^\mu_{ab}\gamma^a\gamma^b) = \gamma_0\partial_t + \frac{1}{r}[\gamma^3\partial_{\log(r)} + \gamma^1\partial_\theta$$
$$+ \frac{\gamma^2}{\sin\theta}\partial_\phi + \gamma^3 + \frac{\gamma^1\cot\theta}{2}] . \tag{B2}$$

The static approximation removes the γ_0 reducing it to 3D. The radial quantization on $\mathbb{R} \times \mathbb{S}^2$ rescales the fields $(\psi \to r^{-1}\psi, \bar{\psi} \to r^{-1}\bar{\psi})$, placing the 2D Dirac action on the unit $\mathbb{S}^2$ given by

$$S = \int \sin\theta d\theta d\phi \, \bar{\psi}[\gamma^1(\partial_\theta + \frac{\cot\theta}{2}) + \frac{1}{\sin\theta}\gamma^2\partial_\phi]\psi . \tag{B3}$$

This is two copies of 2 component fermions with action,

$$S = \int \sin\theta d\theta d\phi \bar{\psi}(\sigma^\mu \boldsymbol{D}_\mu + m)\psi \tag{B4}$$

$$= \int \sin\theta d\theta d\phi \, \bar{\psi}[\sigma^1(\partial_\theta + \frac{\cot\theta}{2}) + \frac{1}{\sin\theta}\sigma^2\partial_\phi]\psi,$$

in agreement with Eq. (80), as promised. The term $\frac{1}{2}\cot\theta$ corresponds to a spin connection on $\mathbb{S}^2$. Defining

$$\nabla = \sigma^1(\partial_\theta + \cot\theta/2) + \frac{1}{\sin\theta}\sigma^2\partial_\phi , \tag{B5}$$

we turn next to the spectrum, $\nabla\psi = i\lambda\psi$, of the massless Dirac operator [28, 39, 40] on $\mathbb{S}^2$.

For the positive spectrum, $\lambda_+ > 0$, the eigen-functions are designated by $\xi_+(\theta,\phi)$. The analysis can be done by the usual procedure, by seperation of variables and Fourier expansion of the spinor $\xi_+(\theta,\phi)$ in ϕ, $\xi_+(\theta,\phi) = \sum_m e^{-im\phi}f_+(\theta)$, leading to a first order ordinary differential equation in θ for a two-component spinor $f_+(\theta)$. It can be shown that spinors in this gauge are anti-periodic in ϕ and $m = n + 1/2$ takes on half-integral values. This leads to a coupled first order ODE between its upper and lower components, which after one iteration gives an ordinary second order ODE separately for the upper and the lower component.

By imposing a normalizability condition on $f_+(\theta)$, the discrete spectrum can be found, with eigenvalues,

$$\lambda_+ = j + 1/2 , \tag{B6}$$

where $j = 1/2, 3/2, \cdots$ and $-j \leq m \leq j$. That is, for each λ_+, there is a $(2j+1)$-fold degeneracy due to rotational invariance. The corresponding wave functions can be expressed in terms of Jacobi polynomials, $P_n^{(\alpha,\beta)}$,

$$\xi_{+,(j,m)}(\theta,\phi) = C^+_{jm} e^{im\phi} \tag{B7}$$
$$\times \begin{pmatrix} \sin^m(\theta/2)\cos^{m+1}(\theta/2)P_{j-m}^{(m-\frac{1}{2},m+\frac{1}{2})}(\cos\theta) \\ i\,\sin^{m+1}(\theta/2)\cos^m(\theta/2)P_{j-m}^{(m+\frac{1}{2},m-\frac{1}{2})}(\cos\theta) \end{pmatrix} .$$

The eigenfunctions corresponding to the negative eigenvalues, λ_-, can be obtained via $\xi_{-,(j,m)}(\theta,\phi) = i\sigma_3\phi_{+,(j,m)}$. For the record, we note that these wave functions are normalized so that

$$\int_{S^2}\sin\theta d\theta d\phi\, \xi_{\epsilon,(j,m)}^{\dagger}\xi_{\epsilon',(j',m')} = \delta_{\epsilon,\epsilon'}\delta_{j,j'}\delta_{m,m'}, \quad \text{(B8)}$$

with C_{jm}^+ given in Ref. [28].

By performing a local rotation, it is also possible to express these wave functions in terms of the usual spherical harmonics, Y_{lm} [28]. Introducing $\Phi^{\pm}(j,m) = V^{\dagger}\xi_{\pm}$, where $V^{\dagger} = e^{i\theta\sigma_2/2}e^{-i\phi\sigma_3/2}$, one finds that

$$\Phi^{\pm}(j,m) = \frac{(1\pm i)}{2} \quad \text{(B9)}$$

$$\times \begin{pmatrix} \sqrt{\frac{(l+m)}{4l}}Y_{j^-,m^-}(\theta,\phi) \mp i\sqrt{\frac{(j-m+1)}{4(j+1)}}Y_{j^+,m^-}(\theta,\phi) \\ \sqrt{\frac{(j-m)}{4j}}Y_{j^-,m^+}(\theta,\phi) \pm i\sqrt{\frac{(j+m+1)}{4(j+1)}}Y_{j^+,m^+}(\theta,\phi) \end{pmatrix}$$

where $j^{\pm} = j \pm \frac{1}{2}$ and $m^{\pm} = m \pm \frac{1}{2}$.

Finally let's give a direct evaluation of the Lichnerowicz formula,

$$-\nabla^2 = -\frac{1}{\sqrt{g}}\boldsymbol{D}_{\mu}\sqrt{g}g^{\mu\nu}\boldsymbol{D}_{\nu} + \frac{1}{2}\sigma^{ab}e_a^{\mu}e_b^{\nu}\boldsymbol{R}_{\mu\nu}, \quad \text{(B10)}$$

in Eq. (50).

On $\mathbb{S}^2$ the operator,

$$-\nabla^2 = -[\,\partial_{\theta}^2 + \cot\theta\partial_{\theta} + \frac{1}{\sin^2\theta}\partial_{\phi}^2 - i\sigma_3\frac{\cos\theta}{\sin^2\theta}\partial_{\phi}$$
$$- \frac{1}{4\sin 2\theta} - \frac{1}{4}\,], \quad \text{(B11)}$$

has spectrum $(j+1/2)^2$, which is naturally the absolute value square of the Dirac operator spectrum $\pm i(j+1/2)$. It follows that in 2D the covariant spinor Laplacian alone, which is the first term in the Lichnerowicz formula (B10), has eigenvalues, $(j+1/2)^2 - 1/2 = j(j+1) - 1/4$ in accord with our numerical evaluation of the Wilson term (86) in Sec. V A.

[1] T. Appelquist, R. Brower, S. Catterall, G. Fleming, J. Giedt, A. Hasenfratz, J. Kuti, E. Neil, and D. Schaich, in *Community Summer Study 2013: Snowmass on the Mississippi (CSS2013) Minneapolis, MN, USA, July 29-August 6, 2013* (2013) arXiv:1309.1206 [hep-lat].

[2] R. Brower, G. Fleming, and H. Neuberger, Phys.Lett. **B721**, 299 (2013), arXiv:1212.6190 [hep-lat].

[3] R. C. Brower, M. Cheng, and G. T. Fleming, PoS **LATTICE2013**, 335 (2014), arXiv:1407.7597 [hep-lat].

[4] R. C. Brower, M. Cheng, and G. T. Fleming, PoS **LATTICE2014**, 318 (2015).

[5] R. C. Brower, G. Fleming, A. Gasbarro, T. Raben, C.-I. Tan, and E. Weinberg, in *Proceedings, 33rd International Symposium on Lattice Field Theory (Lattice 2015)* (2016) arXiv:1601.01367 [hep-lat].

[6] T. Regge, Nuovo Cim. **19**, 558 (1961).

[7] H. W. Hamber, Gen. Rel. Grav. **41**, 817 (2009), arXiv:0901.0964 [gr-qc].

[8] G. Strang and G. Fix, *An Analysis of the Finite Element Method 2nd Edition*, 2nd ed. (Wellesley-Cambridge, 2008).

[9] M. Desbrun, A. N. Hirani, M. Leok, and J. E. Marsden, ArXiv Mathematics e-prints (2005), math/0508341.

[10] N. H. Christ, R. Friedberg, and T. D. Lee, Nucl. Phys. **B210**, 337 (1982).

[11] N. H. Christ, R. Friedberg, and T. D. Lee, Nucl. Phys. **B202**, 89 (1982).

[12] N. H. Christ, R. Friedberg, and T. D. Lee, Nucl. Phys. **B210**, 337 (1982).

[13] R. C. Brower, M. Cheng, E. Weinberg, G. T. Fleming, A. D. Gasbarro, T. Raben, and C.-I. Tan, "Quantum Finite Elements for Scalar Field Theory on the Riemann Sphere," (2016), in preparation.

[14] E. H. Spanier, McGraw-Hill.

[15] R. Friedberg, T. D. Lee, and H.-c. Ren, Prog. Theor. Phys. Suppl. **86**, 322 (1986).

[16] T. Banks, Y. Dothan, and D. Horn, Phys. Lett. **B117**, 413 (1982).

[17] S. Watterson and J. Sexton, *Proceedings, 23rd International Symposium on Lattice field theory (Lattice 2005): Dublin, Ireland, Jul 25-30, 2005*, PoS **LAT2005**, 277 (2006), arXiv:hep-lat/0510052 [hep-lat].

[18] W. A. Miller, Class. Quant. Grav. **14**, L199 (1997), arXiv:gr-qc/9708011 [gr-qc].

[19] H.-c. Ren, Nucl. Phys. **B301**, 661 (1988).

[20] H. W. Hamber, (2007), arXiv:0704.2895 [hep-th].

[21] L. Bogacz, Z. Burda, J. Jurkiewicz, A. Krzywicki, C. Petersen, and B. Petersson, *Theoretical physics. Proceedings, 41st Cracow School, Zakopane, Poland, June 2-11, 2001*, Acta Phys. Polon. **B32**, 4121 (2001), arXiv:hep-lat/0110063 [hep-lat].

[22] L. Bogacz, Z. Burda, C. Petersen, and B. Petersson, Nucl. Phys. **B630**, 339 (2002), arXiv:hep-lat/0107015 [hep-lat].

[23] Z. Burda, J. Jurkiewicz, and A. Krzywicki, Phys. Rev. **D60**, 105029 (1999), arXiv:hep-lat/9905015 [hep-lat].

[24] M. Caselle, A. D'Adda, and L. Magnea, Phys. Lett. **B232**, 457 (1989).

[25] L. Brewin, Class. Quant. Grav. **15**, 3085 (1998), arXiv:gr-qc/9701057 [gr-qc].

[26] C. J. Isham and C. N. Pope, Phys. Lett. **B114**, 137 (1982).

[27] L. Brewin, Class. Quant. Grav. **26**, 175017 (2009), arXiv:0903.2087 [gr-qc].

[28] A. A. Abrikosov, Jr., (2002), arXiv:hep-th/0212134 [hep-th].

[29] A. Chodos and J. B. Healy, Nucl. Phys. **B127**, 426 (1977).

[30] W. Celmaster and F. Krausz, Nucl. Phys. **B220**, 434 (1983).

[31] R. Narayanan and H. Neuberger, Nucl. Phys. **B412**, 574 (1994), arXiv:hep-lat/9307006 [hep-lat].

[32] P. Christe and M. Henkel, Lect. Notes Phys. **M16**, 1 (1993), arXiv:cond-mat/9304035 [cond-mat].

[33] S. Rychkov, (2016), arXiv:1601.05000 [hep-th].

[34] Y. Shamir, in *Lattice fermions and structure of the vacuum. Proceedings, NATO Advanced Research Workshop, Dubna, Russia, October 5-9, 1999* (1999) pp. 27–39, arXiv:hep-lat/9912027 [hep-lat].

[35] R. C. Brower, H. Neff, and K. Orginos, (2012), arXiv:1206.5214 [hep-lat].

[36] I. Jack and H. Osborn, Nucl. Phys. **B234**, 331 (1984).

[37] I. Jack and H. Osborn, Nucl. Phys. **B249**, 472 (1985).

[38] N. Christ, R. Friedberg, and T. Lee, Nucl.Phys. **B202**, 89 (1982).

[39] V. M. Villalba, Eur. J. Phys. **15**, 191 (1994), arXiv:hep-th/9405033 [hep-th].

[40] R. Camporesi and A. Higuchi, J. Geom. Phys. **20**, 1 (1996), arXiv:gr-qc/9505009 [gr-qc].